

MIT Open Access Articles

Gamma entrainment using audiovisual stimuli alleviates chemobrain pathology and cognitive impairment induced by chemotherapy in mice

The MIT Faculty has made this article openly available. **Please share** how this access benefits you. Your story matters.

Citation: TaeHyun Kim et al. ,Gamma entrainment using audiovisual stimuli alleviates chemobrain pathology and cognitive impairment induced by chemotherapy in mice.Sci. Transl. Med.16,eadf4601(2024).

As Published: 10.1126/scitranslmed.adf4601

Publisher: American Association for the Advancement of Science (AAAS)

Persistent URL: <https://hdl.handle.net/1721.1/153638>

Version: Author's final manuscript: final author's manuscript post peer review, without publisher's formatting or copy editing

Terms of use: Creative Commons Attribution-Noncommercial-ShareAlike;Attribution-NonCommercial-ShareAlike 3.0 Unported



1 **Title: Gamma entrainment using sensory stimuli alleviates chemobrain pathology and**
2 **cognitive impairment induced by chemotherapy agents**

3 **Authors:** TaeHyun Kim¹, Benjamin T. James², Martin C. Kahn¹, Cristina Blanco-Duque¹,
4 Fatema Abdurrob¹, Md Rezaul Islam¹, Nicolas S. Lavoie¹, Manolis Kellis^{2,4}, Li-Huei Tsai^{1,3,4*}

5 **Affiliations:**

6 ¹Picower Institute for Learning and Memory, Massachusetts Institute of Technology, Cambridge,
7 MA, USA.

8 ²Computer Science and Artificial intelligence Laboratory, Massachusetts Institute of
9 Technology, Cambridge, MA, USA.

10 ³Department of Brain and Cognitive Sciences, Massachusetts Institute of Technology,
11 Cambridge, MA, USA.

12 ⁴Broad Institute of Harvard and MIT, Cambridge, MA, USA

13 *Corresponding author. Email: lhstai@mit.edu

14

15 **One Sentence Summary:** GENUS treatment given with chemotherapy attenuates chemobrain
16 pathology and rescues cognitive impairment in mouse models.

17

18 **Abstract:** Cancer patients undergoing chemotherapy frequently experience a neurological
19 condition known as chemotherapy-related cognitive impairment, or ‘chemobrain’, which can

20 persist for the remainder of their lives. Despite the growing prevalence of chemobrain, both its
21 underlying mechanisms and treatment strategies remain poorly understood. Recent findings
22 suggest that chemobrain shares several characteristics with neurodegenerative diseases, including
23 chronic neuroinflammation, DNA damage, and synaptic loss. We investigated whether Gamma
24 ENtrainment Using Sensory stimuli (GENUS), which has been shown to alleviate aberrant
25 immune and synaptic pathologies in mouse models of neurodegeneration, could also mitigate
26 chemobrain phenotypes. When administered concurrently with the chemotherapeutic agent
27 cisplatin, GENUS alleviated cisplatin-induced pathology, promoted oligodendrocyte survival, and
28 improved cognitive functions in a mouse model of chemobrain. Importantly, these effects persisted
29 up to 105 days post-GENUS treatment, suggesting the potential for long-lasting benefits. *However,*
30 *when treated 90 days post-chemotherapy, GENUS only provided limited benefits indicating*
31 *GENUS is most effective when used to prevent the progression of chemobrain pathology.*
32 Furthermore, we demonstrated that the effects of GENUS are not limited to cisplatin-induced
33 chemobrain, but also extend to methotrexate (MTX)-induced symptomology. Collectively, these
34 findings suggest that GENUS may represent a versatile treatment approach for a broad spectrum
35 of chemobrain patients.

36 **Main Text:**

37 **INTRODUCTION**

38 Chemotherapy has improved survival rates and life expectancy for patients, but it often comes with
39 considerable side effects. One such side effect is chemotherapy-related cognitive impairment, or
40 'chemobrain', which is characterized by short-term memory loss, attention deficit, and chronic

41 fatigue(1). More complex cognitive functions, such as executive functioning and multitasking,
42 may be affected for months or even years after treatment ends, impacting quality of life(1).
43 Although the condition was recognized more than 40 years ago, our understanding of the molecular
44 and cellular mechanisms underlying chemobrain, as well as effective treatment strategies, remain
45 limited.

46 Chemotherapeutic agents can cause DNA damage and epigenetic modification(4) in various
47 brain cells, leading to altered gene expression or even cell death. Additionally, chronic
48 upregulation of pro-inflammatory signals outside the brain, either from peripheral immune
49 responses to cancer cells or secondary effects of cancer treatments(4), can lead to activation of
50 glial cells within the brain. Recent studies suggest that chemobrain may be caused by chronic
51 activation of glial cells such as microglia and astrocytes, resulting in dysregulation of brain
52 network formation(5).

53 Pharmacological treatments for chemobrain have primarily focused on common pathologies
54 such as white matter damage and neurodegeneration(6). Multiple studies have detected
55 demyelination due to loss of oligodendrocytes in chemobrain, highlighting the vulnerability of
56 these cells and their precursors to chemotherapeutic agents. Recent research in chemobrain animal
57 models showed that a persistent pro-inflammatory state of microglia led to incomplete maturation
58 of oligodendrocyte precursor cells (OPCs) into oligodendrocytes(5) and disrupts neuron-
59 oligodendrocyte communication(7). While restoring the myelin sheath or preventing myelin loss
60 due to reactive glia successfully rescued cognitive impairment in chemobrain model animals(5, 7–
61 9), there are currently no effective therapeutic options for humans(6).

62 GENUS is a non-invasive sensory stimulation technique that uses light flickering or sound
63 pulsating at 40 Hz to induce 40 Hz neural activity. Neural activity in the 40 Hz range is thought to
64 relate to cognitive functions such as attention and memory and are altered in cognitive disorders
65 like Alzheimer's disease (AD)(10). GENUS treatment has been shown to attenuate AD pathologies
66 in several different mouse models of AD(11–15). GENUS also altered the activation state of glial
67 cells such as microglia and astrocytes in both AD mouse models and healthy mice(11–14, 16) and
68 provided neuroprotective effects in an ischemic brain mouse model(17). Based on animal model
69 studies, GENUS holds high potential as a non-invasive therapy for neurodegenerative disorders.
70 Indeed, early clinical trials show GENUS to be safe and tolerable in both cognitively normal
71 subjects and patients with mild AD(18–20). Given the neurodegenerative nature of chemobrain,
72 we decided to test if GENUS can ameliorate chemobrain pathology and rescue cognitive
73 impairment in two different mouse models of chemobrain with cisplatin- or MTX-induced
74 symptomology.

75 **RESULTS**

76 **GENUS entrains cisplatin-induced chemobrain mouse model**

77 We first examined whether GENUS could induce 40 Hz neural activity in a widely-used cisplatin-
78 based mouse model of chemobrain. This model was created using an intraperitoneal (i.p.) cisplatin
79 injection schedule that mirrors clinical chemotherapy practices(8, 9). Given the association
80 between cisplatin treatment and sensory impairments such as hearing loss and vision damage(21,
81 22), we sought to confirm that cisplatin-treated animals could still exhibit 40 Hz neural activity in
82 response to auditory and visual stimuli. For this purpose, animals were implanted with three

83 electroencephalogram (EEG) screws, evenly distributed between the visual cortex and the
84 prefrontal cortex (PFC) – regions crucial for executive functioning(23), which is often
85 compromised in chemobrain patients. Following a two-week recovery period post-surgery, the
86 animals were administered two five-day courses of 2.3 mg/kg cisplatin injections, with a five-day
87 break in between, to induce chemobrain. On day 21, EEG recordings of the local field potential
88 (LFP) revealed power spectral density (PSD) peaks at 40 Hz across all three monitored cortex
89 areas during GENUS stimulation (red vs black lines in **Fig. 1A**) and exclusively during the period
90 of GENUS stimulation (**Fig. 1B**). These findings confirm the GENUS induces 40 Hz neural
91 activity following cisplatin treatment.

92 **GENUS ameliorates neurodegenerative pathology in a chemobrain mouse model**

93 Previous studies have demonstrated that GENUS treatment can modify neurodegenerative
94 pathologies in AD mouse models (6). To investigate whether GENUS exerts a similar influence
95 in a chemobrain mouse model, we administered combined visual and auditory GENUS for one
96 hour daily, during and after the cisplatin administration period (**Fig. 1C**). We monitored body
97 weight as a general health marker. Animals treated with cisplatin exhibited significant body
98 weight loss, while control animals treated with PBS did not. However, GENUS did not
99 significantly affect body weight in either group (**fig. S1**).

100 We first established that cisplatin-treated animals that had not received GENUS (Cis NS,
101 for Cisplatin No Stimulation) had significant expansion of the lateral ventricles compared to
102 control PBS-treated animals with (S, for Stimulation) or without (NS) GENUS (**Figs. 1D, E**). Cis
103 S animals had similar ventricle size with PBS controls. Similar effects were seen for changes in

104 the volume of white matter above the lateral ventricle. Corpus callosum in the Cis NS group was
105 significantly thinner compared to the other groups (**figs. S2A, B**), suggesting that GENUS prevents
106 brain atrophy and white matter loss associated with cisplatin treatment (**Figs. 1D, E**).

107 We subsequently evaluated neuronal damage in our chemobrain mouse model. We
108 focused on the hippocampal CA1 and PFC areas given their well-documented importance in
109 numerous relevant cognitive functions and their known susceptibility to chemotherapy(24, 25).
110 Our findings revealed that cisplatin treatment significantly increased the DNA-damage marker
111 γ H2AX⁺ cells compared to PBS treatment, and that GENUS treatment prevented this increase
112 (**Figs. 1F, G**). Furthermore, we observed a significant reduction in the number of NeuN⁺ cells in
113 both the CA1 and PFC areas following cisplatin treatment (**fig. S2C**). GENUS stimulation
114 rescued [this loss of NeuN](#) cells the CA1 (**figs. S2D**), but not in the PFC (**fig. S2E**). These results
115 suggest that GENUS stimulation in cisplatin-treated animals may provide region-specific
116 protection against chemotherapy-induced DNA damage and neuronal loss.

117 Due to their mitotic nature, stem cell populations are susceptible to DNA damage during
118 chemotherapy. Reduced neurogenesis in the hippocampus has been proposed as a contributing
119 factor to cognitive impairment in chemobrain(25). Indeed, when we used Sox2 as a marker for
120 neural stem cells (NSCs) or neural progenitor cells (NPCs), we observed a higher number of
121 NSC/NPC with DNA damage in the dentate gyrus of the Cis NS group compared to PBS
122 controls (**figs S2F, G**), as well as a lower number of NSC/NPC (**fig. S2H, I**). GENUS treatment
123 rescued both alterations (**figs. S2G, I**). GENUS also increased the proliferating cell population
124 marked by Ki67 in both PBS and cisplatin-treated groups (**figs. S2H, J**). Also, the number of

125 Ki67⁺ Sox2⁺ cells in the PBS group was higher, although the difference compared to other
126 groups was not significant (**figs. S2J, K**). In contrast, GENUS did cause significant increases in
127 the number of immature neurons in both PBS and cisplatin-treated conditions (**figs. S2H, L**).
128 Together, these findings suggest that GENUS can prevent the loss of NSC/NPC populations due
129 to DNA damage and promote hippocampal neurogenesis.

130 Cisplatin treatment in mouse models has been shown to cause neurite and synaptic
131 loss(26). We investigated if GENUS could also protect neurons from losing synaptic connections
132 after cisplatin treatment(26). Cisplatin treatment reduced the excitatory synaptic marker vGlut1
133 in both the PFC (**figs. S3A, C**) and CA1 (**Figs. S3D, F**), while the inhibitory synaptic marker
134 VGAT remained unaffected (**figs. S3A, B, D, E**). Within the PFC region, GENUS treatment
135 increased the intensities of both VGAT and vGlut1 in PBS-administered animals. However, only
136 the VGAT intensity increased in the cisplatin-administered cohort (**figs. S3D, F**). These
137 observations suggest that, under normal physiological conditions, GENUS treatment has the
138 potential to bolster both excitatory and inhibitory synaptic connections. However, in the context
139 of cisplatin administration, GENUS seems to be less effective in enhancing excitatory synapses.

140 Chronic inflammatory glial activation has been proposed as an underlying cause of
141 chemobrain in an MTX-induced mouse model(5). To determine whether cisplatin treatment also
142 results in glial activation, we evaluated the numbers of microglia and astrocytes in the
143 hippocampal CA1 region along with the microglial activation marker CD68 and the reactive
144 astrocyte marker C3 (**Fig. 1H, figs. S4A**). Cis NS animals indeed exhibited increased numbers of
145 Iba1⁺ microglia and GFAP⁺ astrocytes, as well as increased microglial CD68 or astrocytic C3

146 expression compared to PBS-treated animals (**Fig. 1H-K, figs. S4A-C**). Remarkably, Cis S
147 animals did not show a significant increase in any of these measures of glial activation (**Figs.**
148 **1H-K, figs. S4A-C**). In the PFC, we observed similar microglial behavior as in the CA1 region
149 (**figs. S4D-F**), but we did not detect increased GFAP or GFAP/C3 co-expressing cells following
150 cisplatin treatment (**figs. S4G-I**). When we stained for microglia in the corpus callosum, we
151 observed similar effects to those seen in the hippocampal CA1 area, specifically that GENUS
152 mitigated the increased number of Iba1⁺ microglia (**figs. S4J, K**) and CD68 expression (**figs.**
153 **S4J, L**). These findings suggest that cisplatin treatment induces glial activation and, crucially,
154 that GENUS treatment can alleviate this activation.

155 **GENUS protects the brain from cisplatin-induced demyelination**

156 Demyelination of neuronal axons is one of the best characterized pathologies in cisplatin-induced
157 chemobrain mouse models(8, 9). Consequently, we investigated whether GENUS treatment
158 could influence the integrity of the myelin sheath in chemobrain mice. Using transmission
159 electron microscope (TEM) images of the corpus callosum (**Fig. 1L**), we assessed the myelin
160 sheath thickness. Our findings revealed that Cis NS animals exhibited a significantly higher g-
161 ratio (**Figs. 1L, M**) and fewer myelinated axons (**Figs. 1L, N**) compared to PBS-treated groups.
162 In contrast, Cis S animals demonstrated g-ratios (**Fig. 1M**) and numbers of myelinated axons
163 (**Fig. 1N**) comparable to those of animals in the PBS groups. In the PFC, staining for myelin
164 basic protein (MBP) showed significantly lower myelin coverage in Cis NS animals. However,
165 this reduction was not observed in Cis S animals (**figs. S5A, B**). We further confirmed that the
166 MBP staining represented axonal myelin by co-staining with neurofilament. We did not observe

167 any difference in the colocalization of MBP and neurofilament staining across all four groups
168 (**figs. S5C, D**). These findings suggest that GENUS is capable of mitigating cisplatin-induced
169 demyelination.

170 **GENUS promotes cisplatin-resistance gene expression**

171 To get a better understanding of how GENUS-induced gene expression changes in different
172 brain cells help to alleviate chemobrain symptoms, we performed single-cell RNA sequencing
173 (scRNA-seq). As previously described, we generated the cisplatin-induced chemobrain mouse
174 model and treated it with either GENUS or control light and sound. After 21 days of GENUS
175 stimulation, we collected hippocampi and prepared cDNA libraries for scRNA-seq. Following
176 rigorous quality control measures, a dataset comprising 19,834 single-cell transcriptomes was
177 curated. These transcriptomes were categorized into 12 distinct clusters post normalization (**Fig.**
178 **2A, Methods**). We were able to map these clusters to major cell types based on marker gene
179 expression (**fig. S6A**). We observed no significant difference in cell type abundance across
180 animals treated with cisplatin or PBS, regardless of the presence or absence of GENUS (**fig.**
181 **S6B, C**).

182 We first looked at the total number of differentially expressed genes (DEGs) across cell
183 types to determine which cell type was most affected by cisplatin treatment and by GENUS. We
184 found that cisplatin treatment caused the highest number of DEGs in oligodendrocytes (**Fig. 2B,**
185 **fig. S7A, Cis NS vs PBS NS**), confirming prior reports that oligodendrocytes and OPC are
186 particularly sensitive to chemotherapeutic toxicity(2, 5). GENUS treatment had little effect on
187 any cell type in PBS-treated animals (**fig. S7A, PBS S vs PBS NS**), but in cisplatin-treated

188 animals induced the highest number of DEGs again in oligodendrocytes (**Fig. 2B, fig. S7A**, Cis S
189 vs Cis NS). To explore the effect of GENUS treatment on oligodendrocyte gene expression after
190 cisplatin treatment in more detail, we compared specific DEGs in Cis S vs. Cis NS
191 oligodendrocytes. We found that genes known to provide protective effects against or to be
192 involved in repair of cisplatin-induced damage (*Cdkn1a*, *Ddit4*, *Mt1*) and genes known to be
193 related to anti-inflammatory pathways and cell survival in the context of cisplatin treatment
194 (*Sgk1*, *Sgk3*, *Hif3a*, *Pla2g3*, *Nfkbia*) were upregulated in Cis S compared to Cis NS. Conversely,
195 genes related to oligodendrocyte apoptosis from oxidative stress (*Jun*, *Egr1*, *Fos*, *JunB*, *FosB*,
196 *Dusp1*, *Lars2*) were downregulated in Cis S compared to Cis NS (**Fig. 2C**). We also found that
197 genes related to the Gene Ontology (GO) terms “ATP biosynthetic process”, “ATP synthesis
198 process”, “oxidative phosphorylation”, and “aerobic respiration” which are all functions
199 associated with mitochondrial function, were upregulated in Cis S (**Fig. 2D**). This finding
200 indicates that GENUS promotes mitochondrial function in oligodendrocytes, which is important
201 for myelin sheath formation and maintenance, both of which are metabolically demanding
202 processes for oligodendrocytes(27). Conversely, genes related to GO terms “response to
203 chemical” and “regulation of apoptotic process” were downregulated (**Fig. 2D**), indicating that
204 GENUS treatment protected oligodendrocytes from cisplatin cytotoxicity. Specifically, we found
205 that GENUS treatment promoted expression of genes involved in negative regulation of
206 apoptotic process (GO:0043069) but did not have much effect on expression of genes involved in
207 positive regulation of apoptotic process (GO:0043065) (**Fig. 2E, fig. S7B**). These results suggest
208 that GENUS treatment protected oligodendrocytes from apoptotic processes in response to
209 cisplatin treatment.

210 Since our histological data show that GENUS treatment alters microglia and astrocyte
211 responses to cisplatin treatment, we next analyzed DEGs in these cell types for Cis S vs Cis NS.
212 In Cis S microglia, we found the cisplatin resistance gene *Ddit4* and genes involved in protein
213 translation (*Rpl10-ps3*, *Rps27rt*, *Rpl23a*, *Pabpc1*) to be upregulated, while genes involved in
214 inflammatory signaling (*Atf3*, *Fos*, *Ccr5*, *Klf6*, *Gstp1*) were downregulated (**fig. S8A**). We also
215 found that GO terms related to protein translation such as “organonitrogen compound
216 biosynthetic process”, “cellular macromolecule biosynthetic process”, “cellular amide metabolic
217 process” and “cellular nitrogen compound metabolic process” were upregulated in Cis S
218 microglia, while “cellular response to chemical stimulus” was downregulated (**fig. S8C**).
219 Increased gene expression related to protein translation is observed in phagocytic microglia in
220 AD model mice(28), and phagocytic activity of microglia contributes to tissue homeostasis(29,
221 30) and re-establishment of myelin sheaths in demyelinating diseases by clearing the myelin
222 debris(31, 32). Together, our data suggest that transcriptional alterations in microglia after
223 GENUS treatment are linked to a neuroprotective function.

224 In our analysis of DEGs between Cis S and Cis NS astrocytes, we observed an
225 upregulation of genes involved in the repair of cisplatin-induced oxidative damage (*Mt1*, *Mt2*).
226 In contrast, genes associated with astrocyte recruitment to injury sites and glial scar formation
227 (*Aqp4*, *Slc6a11*, *Eno1*, *Gpr171l*) were downregulated (**fig. S8B**). We also found that GO terms
228 related to locomotion of the cell and subcellular reorganization of molecules such as “transport,”
229 “localization,” “cell adhesion,” “organic substance transport,” and “regulation of cellular
230 component organization” were downregulated in Cis S astrocytes (**fig. S8D**), consistent with our

231 earlier immunohistochemical finding that GENUS treatment ameliorated astrogliosis in response
232 to cisplatin toxicity.

233 To validate our DEG analysis results in oligodendrocytes, we selected two genes, *Klf9*
234 and *Cdkn1a*, that showed differential upregulation in Cis S vs Cis NS oligodendrocytes. We then
235 analyzed their expression in brain slices. For this, we used an antibody against the Klf9 protein
236 (**Fig. 2F**) and a fluorescent in situ hybridization (FISH) probe for the *Cdkn1a* RNA transcript
237 (**fig. S8E**). We chose *Klf9* for validation given that it mediates oligodendrocyte differentiation
238 and is known to be a key factor in the recovery of the myelin sheath after demyelination(33).
239 *Cdkn1a* was selected for validation because it plays an important role in oligodendrocyte
240 maturation in addition to its well-known involvement in cell cycle regulation and because a
241 previously published single-cell transcriptomic analysis(34) reported *Cdkn1a* as one of the top
242 DEG associated with oligodendrocytes surviving a demyelination event. For both genes, we
243 confirmed the increased expression with GENUS that was indicated by the scRNA-seq results
244 (**Fig. 2G, fig. S8F**). Overall, our scRNA-seq results show that GENUS treatment increases
245 cisplatin-resistance gene expression and reduces inflammatory gene expression in multiple cell
246 types.

247 **GENUS promotes oligodendrocyte survival after cisplatin treatment**

248 Based on the scRNA-seq results, we hypothesized that GENUS treatment might ameliorate
249 demyelination through an effect on the oligodendrocyte population. By staining with marker
250 proteins Olig2 and CC1 to identify oligodendrocytes, we observed that the GENUS treatment
251 decreased oligodendrocyte loss in the corpus callosum area. Compared to the PBS control groups,

252 the loss was reduced from 65% in the Cis NS group to 35% in the Cis S group (**Figs. 3A, B**). This
253 finding indicates that GENUS indeed reduces the damaging effect of cisplatin on oligodendrocytes.

254 Next, we tested whether GENUS reduced oligodendrocyte loss by promoting OPC
255 differentiation to replenish the oligodendrocyte number. In the MTX-induced chemobrain mouse
256 model, it has been reported that OPCs do not fully mature into oligodendrocytes, leading to an
257 increase in OPC numbers(5). We reasoned that if cisplatin treatment also induced an OPC
258 maturation arrest and GENUS increased the number of oligodendrocytes by releasing this arrest,
259 we would see more OPC (Olig2⁺/Pdgfr α ⁺) in Cis NS compared to Cis S. However, we found a
260 depletion of OPCs after cisplatin treatment to similar numbers with or without GENUS (**Figs 3C,**
261 **D**). This finding indicates that GENUS did not replenish oligodendrocytes by promoting their
262 differentiation from existing OPCs. Alternatively, GENUS could have increased new OPC
263 formation and accelerated their maturation into oligodendrocytes, resulting in similar OPC but
264 increased oligodendrocyte numbers. To test this hypothesis, we injected 5-Ethynyl-2-
265 Deoxyuridine (EdU) into the animals during the last 3 days of the 21 day GENUS stimulation
266 period to label oligodendrocytes originating from cells dividing during that time period (**Fig. 3E**).
267 We observed a similar depletion of EdU⁺ oligodendrocytes after cisplatin treatment with or without
268 GENUS (**Figs. 3F, G**). Collectively, these findings argue against an effect of GENUS on the
269 replenishment of oligodendrocytes from newly generated precursor cells.

270 Finally, to determine if GENUS enhanced the survival rate of oligodendrocytes during
271 cisplatin treatment, we stained for apoptotic cells using terminal deoxynucleotidyl transferase
272 dUTP nick end labeling (TUNEL). GENUS stimulation significantly reduced the number of total

273 apoptotic cells (**figs. S8G, H**) and Olig2⁺ apoptotic cells (**Figs. 3H and I**) seen in the corpus
274 callosum area after cisplatin treatment, supporting an effect of GENUS on the ability of
275 oligodendrocytes to survive cisplatin treatment and confirming the findings of the scRNA-seq
276 analysis.

277 **GENUS restores cognitive function in chemobrain animals**

278 Next, we investigated whether these molecular alterations observed after GENUS treatment
279 improved cognitive function in chemobrain animals. An open field test (OFT) was performed prior
280 to cognitive testing to see if cisplatin or GENUS had any effect on the locomotion and anxiety of
281 animals (**Figs. 4A-C**). GENUS did not have any effect on animal locomotion, but cisplatin
282 treatment significantly reduced the distance animals moved during the 10 min OFT test (**Fig. 4B**).
283 This reduced mobility could indicate peripheral neuropathy, a commonly documented side effect
284 in patients receiving cisplatin therapy(35). Conversely, our analysis revealed a pronounced effect
285 of GENUS on the duration animals spent in the central zone of the chamber (**Fig. 4C**). This
286 suggests a potential anxiolytic effect of GENUS, as evidenced by reduced anxiety levels in both
287 PBS and cisplatin-administered cohorts post-GENUS treatment.

288 Short-term memory impairment and attention deficits rank among the most prevalent
289 symptoms experienced by patients with chemobrain(1). To evaluate these symptoms in our
290 chemobrain mouse model, we employed a modified version of the novel object recognition (NOR)
291 test, which has been tailored to be more sensitive to attention and short-term memory deficits (**Fig.**
292 **4D**)(5). We observed that the Cis NS mice showed no preference between a novel and familiar
293 object, whereas the PBS-treated mice clearly favored the novel object. Intriguingly, the Cis S group

294 also demonstrated a marked preference for the novel object, exhibiting a discrimination ratio
295 comparable to the PBS control groups (**Fig. 4E**). This underscores the potential of GENUS
296 treatment in mitigating cisplatin-induced short-term memory deficits in this experimental
297 paradigm.

298 Impaired executive functioning is another key symptom in chemobrain patients(1). In
299 rodents, executive functioning can be assessed with the puzzle box test. This test challenges
300 animals with obstacles of varying difficulty levels to enter their preferred dark chamber(36).
301 Previous studies have shown that cisplatin-induced chemobrain model animals show impaired
302 performance in the puzzle box test(8, 9). To test if GENUS could improve cisplatin-induced
303 impairment in executive functioning, we used three obstacles of increasing difficulty: an open
304 corridor (easy), a corridor buried under sawdust (intermediate), and a door plugged with tissue
305 (hard) (**Fig. 4F**). Without GENUS, cisplatin-treated animals required longer time to enter the dark
306 box compared to PBS controls (**Figs. 4G-I**). GENUS treatment rescued the ability of cisplatin-
307 treated animals to solve the intermediate and hard tasks (**Figs. 4H, I**), but did not increase their
308 performance in the easy task, possibly because their impaired locomotion became rate-limiting
309 (**Fig. 4G**). Together, the cognitive testing results show that GENUS was able to rescue cognitive
310 functions ranging from short term memory to problem solving ability in chemobrain animals.

311 **GENUS treatment during chemotherapy rescues chronic chemobrain pathology**

312 Patients with chemobrain often grapple with the condition for an extended period, which
313 frequently persists for over six months following the cessation of chemotherapy. Therefore, it is
314 important to determine if GENUS treatment during chemotherapy also prevents delayed

315 development of chemobrain after chemotherapy and GENUS treatment have ended. To probe this,
316 we designed experimental cohorts with an extended timeline, spanning up to 133 days post the
317 initial cisplatin administration (**Table 1, Figs. 5, 6**).

318 We concurrently gave cisplatin and GENUS treatment to mice as in previous cohorts but
319 tested the animals 126 days after the first cisplatin injection (**Fig. 5A**). At this timepoint, we did
320 not observe any effect of cisplatin or GENUS treatment on locomotion (**Fig. 5B**) or anxiety (**Fig.**
321 **5C**) as determined by the OFT. However, Cis NS animals were still unable to discriminate novel
322 and familiar objects in the NOR test (**Fig. 5D**). Cisplatin treated animals performed comparable to
323 PBS controls in easy (**Fig. 5E**) and intermediate (**Fig. 5F**) task, but required more time to overcome
324 the hard puzzle box obstacle (**Fig. 5G**), demonstrating prolonged cognitive impairment after
325 cisplatin treatment. Cognitive deficits in both NOR and puzzle box were rescued in the Cis S
326 groups, indicating a long lasting effect of GENUS treatment (**Fig. 5D, G**).

327 Next, we investigated chemobrain pathology. In the Cis NS group, demyelination (**Figs.**
328 **5H, I**), a reduction in mature oligodendrocytes (**Figs. 5J, K**), an increase in microglia number and
329 activation state in CA1 and corpus callosum (**Figs. 5M, N, figs. S9B-D**), and an increase in
330 astrocyte number and activation state in CA1 (**Figs. 5P-R**) persisted at 133 days after the start of
331 cisplatin treatment, showing the prolonged effects of chemobrain. In the Cis S group, myelination
332 (**Figs. 5H, I**), oligodendrocyte numbers (**Figs. 5J, K**), and microglia numbers (**Figs. 5M, N, figs.**
333 **S9B, C**), were normalized, while microglial activation state (**Figs. 5M, O and figs. S9B, D**) and
334 astrocyte numbers and activation state were elevated (**Figs. 5P- R**). We found no effect from
335 cisplatin or GENUS treatment on the number of OPC (**Figs. 5J, L**). Finally, we stained for VGAT

336 and vGlut1 as markers of inhibitory and excitatory synapses. In both PFC (**figs. S9E-G**) and
337 CA1(**figs. S9H-J**), cisplatin treatment increased VGAT intensity (**figs. S9F, I**) but reduced vGlut1
338 intensity (**figs. S9G, J**). Notably, GENUS treatment did not exhibit any discernible effect on these
339 changes.

340 In summary, our results indicate that GENUS treatment during cisplatin chemotherapy
341 can prevent cognitive impairment and reduce many chemobrain pathologies. However, certain
342 pathologies, like glial activation and synaptic loss, may re-emerge after the cessation of GENUS
343 treatment (**Table 1**).

344 **GENUS treatment post chemotherapy provides limited effect on chemobrain pathology**

345 Unlike patients with other neurodegenerative conditions, cancer patients know exactly
346 when chemotherapy and thus their risk of developing chemobrain starts. Therefore, it would be
347 possible for new patients to follow our study design and receive GENUS treatment during
348 chemotherapy. However, it is unclear if patients who have already undergone chemotherapy and
349 still suffer from chemobrain could benefit from GENUS treatment. To answer this question, we
350 first treated a cohort of mice with cisplatin and then gave GENUS treatment from day 105 (**Fig.**
351 **6A**). In these mice, we did not observe any effect of cisplatin or GENUS treatment on locomotion
352 (**Fig. 6B**) or anxiety (**Fig. 6C**) during the OFT. Post-chemotherapy GENUS treatment did not
353 rescue the cognitive functions as measured by the NOR test (**Fig. 6D**). Cisplatin treated animals
354 performed comparable to PBS controls in easy (**Fig. 6E**) and intermediate (**Fig. 6F**) tasks, but
355 required more time to overcome the hard puzzle box obstacle (**Fig. 6G**). Unlike the NOR test,
356 GENUS did rescue the ability of cisplatin-treated animals to solve the hard task (**Fig. 6G**). These

357 results suggest that GENUS treatment after chemotherapy can still enhance cognition, but its
358 efficacy is significantly limited.

359 Next, we investigated chemobrain pathology. GENUS treatment three months after
360 cisplatin chemotherapy appeared to ameliorate the demyelination pathology observed after
361 cisplatin treatment (**Figs. 6H, I**), but the difference was not significant between the Cis NS and
362 Cis S groups. GENUS post chemotherapy was also unable to rescue oligodendrocyte loss in corpus
363 callosum (**Figs. 6J-L**); decrease the elevated microglia number in the CA1 (**Figs. 6M, N**); or
364 reduce astrogliosis in CA1 (**Figs. 6P-R**). However, post-chemotherapy GENUS treatment reduced
365 both the Iba1⁺ cell count (**figs. S10B, C**) and the CD68 signal (**figs. S10B, D**) in the corpus
366 callosum of cisplatin-treated animals, as well as the CD68 signal in the CA1 (**Figs. 6M, O**). We
367 found no effect from cisplatin or GENUS treatment on the number of OPC (**Figs. 6J, L**). When
368 we stained for synaptic markers in PFC (**fig. S10E**), we observed a notable increase in VGAT
369 intensity (**fig. S10F**) and a decrease in vGlut1 intensity in response to cisplatin treatment, as
370 compared to the PBS NS group (**fig. S10G**). While GENUS did not influence the cisplatin-treated
371 animals, it did elevate both VGAT (**fig. S10F**) and vGlut1 (**fig. S10G**) intensity in PBS treated
372 animals. In the CA1 region, GENUS treatment appeared to normalize the VGAT intensity in Cis
373 S animals, bringing it on par with the PBS NS group (**figs. S10H, I**). However, there was no
374 discernible effect on the diminished vGlut1 intensity resulting from cisplatin treatment (**figs. S10**
375 **H, J**). These findings hint at a transient impact of GENUS on synapses and microglia. In summary,
376 our data indicate that GENUS has limited efficacy when administered post-chemotherapy (**Table**
377 **1**).

378 **GENUS proves to be effective in another chemobrain mouse model**

379 Next, we tested whether the effect of GENUS was specific to cisplatin-induced chemobrain or also
380 extended to chemobrain caused by a different chemotherapeutic agent. We selected methotrexate
381 (MTX) because it has a different mechanism of action than cisplatin. While cisplatin creates
382 crosslinks with the DNA, damaging and preventing the synthesis of DNA, MTX inhibits the
383 enzyme dihydrofolate reductase (DHFR) and thereby disrupts purine synthesis(37). MTX was
384 administered in a schedule analogous to therapeutic timelines, and GENUS was given from the
385 first day animals received 100 mg/kg MTX (**Fig. 7C**). MTX-treated animals showed slower body
386 weight gain during drug administration, while GENUS had no effect on their body weight during
387 or after the treatment period (**fig. S11A**). We again first tested whether the MTX-induced
388 chemobrain mouse model would show 40 Hz entrainment with sensory stimulation. EEG
389 recordings showed a peak response in power spectral density at 40 Hz (**Figs. 7A, B**).

390 We then investigated the response of MTX-based chemobrain model animals to GENUS
391 treatment based on histological features. Similar to the findings in the cisplatin-induced
392 chemobrain model, we found that demyelination after MTX treatment was rescued by GENUS
393 (**Figs. 7D, E**); that the number of oligodendrocytes was decreased in MTX NS but not in MTX S
394 animals (**Figs. 7F, G**); and that the Iba1 and CD68 signatures were dramatically increased in the
395 corpus callosum of MTX NS but significantly reduced in MTX S (**Figs. 7H-J**).

396 Next, we tested if GENUS could also rescue cognitive impairment in MTX-based
397 chemobrain animals. Unlike cisplatin, MTX did not alter the total distance moved in the OFT,
398 indicating no effect of MTX on animal locomotion (**fig. S11B**). However, the anxiolytic effect of

399 GENUS seen in cisplatin-treated animals was also observed in the MTX model, as an increase in
400 time spent in the center area (**fig. S11C**). In the NOR test assessing short-term memory and
401 attention, MTX-treated animals without GENUS showed no preference between novel and
402 familiar objects. However, MTX-treated animals with GENUS spent significantly more time
403 exploring the novel object, displaying a discrimination ratio similar to the PBS control groups (**Fig.**
404 **7K**). TX animals treated with GENUS outperformed their untreated counterparts in the
405 intermediate and hard puzzle box tasks (**Figs. 7L-N**). These results suggest that the
406 neuroprotective effect of GENUS is not limited to a single chemotherapeutic agent, but can be
407 effective against distinct chemotherapeutic agents that have different mechanisms of action.

408 Next, we tested which behavioral effects and brain pathologies related to MTX-based
409 chemobrain could be detected 133 days after treatment start in the MTX NS and MTX S groups.
410 In the MTX S group, GENUS was administered for 21 days starting from the first day of MTX
411 injection (**figs. S12A, S13A**). We found that MTX treatment reduced the number of mature
412 oligodendrocytes (**figs. S12B, C**) and increased the number of OPC (**figs. S12B, D**). In contrast to
413 our findings in the cisplatin-based chemobrain mouse model, we did not observe any effect of
414 GENUS treatment on the number of oligodendrocytes and OPC (**figs. S12C, D**). When we looked
415 at microglial activation in the CA1 area, we found that MTX increased both the number of Iba1⁺
416 cells (**figs. S12E, F**) and CD68 signal (**figs. S12E, G**) compared to PBS groups. GENUS treatment
417 did not have any effect on the number of Iba1⁺ cells (**figs. S12F**) but significantly decreased CD68
418 signal (**figs. S12G**). The corpus callosum area showed similar trend of increased Iba1⁺ signal (**figs.**
419 **S12H, I**) and CD68 signal (**figs. S12 H, J**) after MTX treatment, and the reduction of CD68 signal

420 after GENUS treatment (**fig. S12J**). Astrocytes showed similar response to MTX and GENUS
421 treatment where the area covered by GFAP signal was increased in both MTX NS and MTX S
422 compared to PBS treated groups (**figs. S12K, L**), GENUS significantly reduced the number of C3⁺
423 GFAP⁺ cells (**figs. S12K, M**). When we measured synaptic markers in this cohort, MTX treatment
424 caused significant reduction of VGAT and vGlut1 intensity in PFC (**figs. S13B-D**) and CA1 area
425 (**figs. S13E-G**), and GENUS treatment rescued VGAT signal intensity in both regions (**figs. S13C,**
426 **F**). These results show that GENUS treatment during MTX chemotherapy rescued inhibitory
427 synaptic loss and partially prevented glial activation even months after the treatment period had
428 ended, while protective effect of GENUS on oligodendrocytes seemed to wear off.

429 Finally, we examined whether post-chemotherapy GENUS treatment could mitigate
430 chemobrain pathology in the MTX model (**figs. S14A, S15A**). We found no effect from GENUS
431 treatment on the number of oligodendrocytes and OPC (**figs. S14B-D**). Also, the number of
432 microglia in the CA1 area(**figs. S14E, F**) was comparable between MTX NS and MTX S, while
433 GENUS treatment significantly reduced CD68 signal (**figs. S14E, G**). In the corpus callosum area,
434 we found MTX treatment increased both Iba1 and CD68 signal, but there were no effect of GENUS
435 treatment (**figs. S14H-J**). We also did not find any effect of GENUS treatment on astrogliosis and
436 astrocytic C3 expression (**figs. S14K-M**). When we measured synaptic markers, we found that
437 only MTX NS had significantly lower VGAT and vGlut1 signal intensity in CA1 area (**figs. S15E-**
438 **G**) compared to PBS NS control group. We did not find any significant effect of GENUS in the
439 PFC area (**figs. S15B-D**). These results show that in the MTX-induced chemobrain model, post-

440 chemotherapy GENUS treatment rescues synaptic loss but provides minimal to no effects on glial
441 activation and oligodendrocyte loss.

442 **DISCUSSION**

443 Proper myelin sheath has an increasingly recognized role in cognitive function(38). Studies in
444 chemobrain animal models have shown that restoration of oligodendrocyte populations and
445 myelin sheaths can ameliorate cognitive impairment(5, 7–9). Our analyses suggest that GENUS
446 rescue demyelination in chemobrain animals and promotes oligodendrocyte survival. Some
447 reports from other demyelinating disease models suggest that surviving oligodendrocytes don't
448 contribute as much myelin as new ones(39). However, our TEM imaging results show that the
449 surviving oligodendrocytes in the Cis S animals form comparable myelin sheaths. The
450 observation that GENUS treatment rescued cognitive impairment also supports that surviving
451 oligodendrocytes are able to maintain a functional myelin sheath.

452 For our transcriptional analyses, we opted for scRNA-seq over single nucleus RNA-seq
453 (snRNA-seq) to capture cytosolic transcripts and to enrich for glial cell types that tend to be
454 underrepresented in snRNA-seq data. Unfortunately, this approach resulted in a trade-off in
455 terms of adequately representing neurons, preventing us from drawing meaningful conclusions
456 about the neuronal transcriptional profile. *However, our histological analysis demonstrate that
457 GENUS can protect neuronal damage and enhance neurogenesis.*

458 While there have been a few successful attempts to rescue cognitive impairment in
459 chemobrain mouse models(5, 6, 8, 9, 40, 41), breakthroughs in treating human patients have
460 been elusive, primarily due to the invasive nature of current treatments. GENUS represents a

461 non-invasive method that has already been demonstrated to be safe in human patients(18, 19),
462 potentially accelerating human trials. It is noteworthy that we observed a beneficial effect of
463 GENUS in both cisplatin and MTX-induced chemobrain mouse models during the early phase of
464 pathology. However, careful consideration should be given to the selection of candidate patients
465 and the timing of GENUS treatment. Our results suggest that GENUS would most benefit
466 patients when administered during chemotherapy to prevent the progression of the pathology,
467 while the benefit would be limited for patients who have already undergone chemotherapy but
468 still exhibit chemobrain symptoms. Unlike other diseases, this preventative approach would suit
469 well for the potential chemobrain patients, as clinicians may schedule GENUS treatment with
470 chemotherapy to cancer patients.

471 have used 21 days of GENUS t Persistent long-term pathology after concurrently
472 administered GENUS differed between the cisplatin-based model and the MTX-based model. In
473 the MTX-based model, the effect of GENUS on oligodendrocytes and microglia seemed to
474 diminish over time, while the excitatory and inhibitory synaptic markers were rescued with
475 GENUS. The varying responsiveness to GENUS across drug models might stem from the
476 distinct molecular mechanisms that lead to similar pathological symptoms. Cisplatin, which can
477 diffuse through the cellular membrane and form cisplatin-DNA crosslinks that inhibit cellular
478 growth and division(42). On the other hand, MTX is taken up by cells through reduced folate
479 carrier 1 (RFC1) and inhibits enzymes such as DHFR and thus purine biosynthesis, impairing
480 DNA replication and repair(43). As MTX competes with folate for the binding sites and cause

481 folate deficiency, which causes microglial inflammatory state(44). Which could have caused
482 relapse of chemobrain symptoms after the cessation GENUS treatment in our study.

483 We have demonstrated 21 days of GENUS stimulation can ameliorate chemobrain
484 pathology in this study. However, it remains a question what the optimal treatment duration is.
485 Prolonging GENUS stimulation beyond the 21 days might enhance the mitigation of chemobrain
486 pathology, and prevent the relapse of the pathology we observed at day 133. It has already been
487 shown in a clinical trial with human AD patients that long-term treatment of GENUS over three
488 months is safe and well-tolerable(20). Therefore, detailed studies on the GENUS treatment
489 timeline would be a valuable future study.

490 Also, before clinical implementation of GENUS, it is crucial to test if there are any
491 frequency specific responses or potential side effects which was not tested in this study. Prior
492 research has highlighted the therapeutic potential of sensory stimulation or transcranial alternating
493 current stimulation (tACS) at 40 Hz in mitigating AD pathology in both animal models and human
494 patients(12–14, 18, 20, 45). Notably, these benefits were not observed at frequencies of 8 or 80
495 Hz. Furthermore, sensory stimulation centered around 40 Hz, but not at 10 or 80 Hz, has been
496 shown to alleviate other neurological conditions, such as ischemic injury(17). This suggests that
497 the 40 Hz frequency might offer therapeutic advantages for a range of neurological disorders.
498 Consistent with these findings, our study revealed that 40 Hz audio and visual stimulation
499 successfully reduced chemobrain pathology. However, given that we have not tested other
500 frequencies in chemobrain, the specificity of the observed effects to the 40 Hz frequency should
501 be tested.

502 **MATERIALS AND METHODS**

503 **Study design**

504 The study aimed to validate whether GENUS can be an effective treatment to chemobrain. Animals
505 were randomly assigned for each experimental group. Animals were purchased from Jaxon lab
506 and randomly assigned to each experimental group. Cisplatin or MTX was given to mice with a
507 schedule analogous to therapeutic timelines. Animals were tested after three weeks or three months
508 from the first chemotherapeutic injection to test the acute pathology and chronic pathology of
509 chemobrain. Experimenter was blinded when analyzing behavior or histological data. All animals
510 were handled and sacrificed as approved by the Massachusetts Institute of Technology Committee
511 on Animal Care (MIT CAC). Power analysis for sample size was not performed prior to the study.
512 All animals in the experiment were included in the data unless specified or the animal was
513 sacrificed/deceased prior to the endpoint of the cohort because of their poor condition after
514 chemotherapy.

515 **Statistical analysis**

516 Data were presented as means \pm SD; level of significance was set at *P < 0.05, **P < 0.01, ***P
517 < 0.001, ****P < 0.0001. Two-way ANOVA was used for statistical analysis of the effect of
518 drug and GENUS, Three-way ANOVA was used for statistical analysis of the effect of drug,
519 GENUS and time. Detailed sample number, replication method and statistical analysis used for
520 each figure are listed on supplemental table S1. All samples or animals were included in the
521 statistical analysis unless otherwise specified.

522

523

524 **Acknowledgement**

525 We would like to thank and acknowledge The JPB Foundation, Lester A. Gimpelson, the Ko
526 Hahn family and many annual fund level donors to MIT's Aging Brain Initiative Fund.

527 **Funding**

528 Manipulating Neural Oscillations with Non-Invasive Sensory Stimulation for Alzheimer's
529 Disease Intervention, NIH-1-R01-AG069232-01A1 (LHT)

530 Ko Hahn Seed Fund, sponsor Melissa Ko Hahn (LHT)

531 MIT cost object#3977800

532 NIH-R01-NS129032, NIH-UG3-NS115064, NIH-R01-AG081017 (MK)

533 **Author contributions:**

534 Conceptualization: THK, LHT

535 Methodology: THK, BTJ, MCK, CDB

536 Investigation: THK, BTJ, MCK, CDB, FA, NSL

537 Visualization: THK, BTJ, MRI

538 Funding acquisition: LHT, MK

539 Project administration: THK, LHT, MK

540 Supervision: LHT, MK

541 Writing – original draft: THK, BTJ, MCK, CDB, FA, LHT

542 **Competing interests:** THK and LHT are coinventors of a patent “Systems, Devices, and Methods
543 for Gamma Entrainment using Sensory Stimuli to Alleviate Cognitive Deficits and/or
544 Neuroinflammation Induced by Chemotherapy Agents.”, Publication number: 20230173295

545 LHT is a scientific cofounder and SAB member of Cognito Therapeutics

546 **Data and materials availability:** All data associated with this study are present in the paper or
547 the Supplementary Materials. scRNA-seq data are deposited at NCBI Gene Expression Omnibus
548 (GEO) under the accession number (GSE216146)

549 **List of Supplementary Materials**

550 Materials and Methods

551 figs. S1 to S15

552 table S1

553 Data Files S1 and S2

554 References (46-51)

555

556 **References and Notes**

- 557 1. M. C. Janelsins, C. E. Heckler, L. J. Peppone, C. Kamen, K. M. Mustian, S. G. Mohile, A. Magnuson,
558 I. R. Kleckner, J. J. Guido, K. L. Young, A. K. Conlin, L. R. Weiselberg, J. W. Mitchell, C. A.
559 Ambrosone, T. A. Ahles, G. R. Morrow, Cognitive Complaints in Survivors of Breast Cancer After
560 Chemotherapy Compared With Age-Matched Controls: An Analysis From a Nationwide, Multicenter,
561 Prospective Longitudinal Study. *J. Clin. Oncol.* **35**, 506–514 (2017).
- 562 2. J. Dietrich, R. Han, Y. Yang, M. Mayer-Pröschel, M. Noble, CNS progenitor cells and
563 oligodendrocytes are targets of chemotherapeutic agents in vitro and in vivo. *J. Biol.* **5**, 22 (2006).
- 564 3. A. Kovalchuk, B. Kolb, Chemo brain: From discerning mechanisms to lifting the brain fog—An aging
565 connection. *Cell Cycle* **16**, 1345–1349 (2017).
- 566 4. X.-M. Wang, B. Walitt, L. Saligan, A. F. Tiwari, C. W. Cheung, Z.-J. Zhang, Chemobrain: A critical
567 review and causal hypothesis of link between cytokines and epigenetic reprogramming associated with
568 chemotherapy. *Cytokine* **72**, 86–96 (2015).
- 569 5. E. M. Gibson, S. Nagaraja, A. Ocampo, L. T. Tam, L. S. Wood, P. N. Pallegar, J. J. Greene, A. C.
570 Geraghty, A. K. Goldstein, L. Ni, P. J. Woo, B. A. Barres, S. Liddelow, H. Vogel, M. Monje,
571 Methotrexate Chemotherapy Induces Persistent Tri-gliaal Dysregulation that Underlies Chemotherapy-
572 Related Cognitive Impairment. *Cell* **176**, 43-55.e13 (2019).
- 573 6. L. D. Nguyen, B. E. Ehrlich, Cellular mechanisms and treatments for chemobrain: insight from aging
574 and neurodegenerative diseases. *EMBO Mol. Med.* **12**, e12075 (2020).
- 575 7. A. C. Geraghty, E. M. Gibson, R. A. Ghanem, J. J. Greene, A. Ocampo, A. K. Goldstein, L. Ni, T.
576 Yang, R. M. Marton, S. P. Paşca, M. E. Greenberg, F. M. Longo, M. Monje, Loss of Adaptive
577 Myelination Contributes to Methotrexate Chemotherapy-Related Cognitive Impairment. *Neuron* **103**,
578 250-265.e8 (2019).
- 579 8. G. S. Chiu, N. Boukelmoune, A. C. A. Chiang, B. Peng, V. Rao, C. Kingsley, H.-L. Liu, A. Kavelaars,
580 S. R. Kesler, C. J. Heijnen, Nasal administration of mesenchymal stem cells restores cisplatin-induced
581 cognitive impairment and brain damage in mice. *Oncotarget* **9**, 35581–35597 (2018).
- 582 9. A. C. A. Chiang, A. V. Seua, P. Singhmar, L. D. Arroyo, R. Mahalingam, J. Hu, A. Kavelaars, C. J.
583 Heijnen, Bexarotene normalizes chemotherapy-induced myelin decompaction and reverses cognitive and
584 sensorimotor deficits in mice. *Acta Neuropathol. Commun.* **8**, 193 (2020).
- 585 10. D. Chan, H.-J. Suk, B. Jackson, N. P. Milman, D. Stark, S. D. Beach, L.-H. Tsai, Induction of specific
586 brain oscillations may restore neural circuits and be used for the treatment of Alzheimer’s disease. *J.*
587 *Intern. Med.* **290**, 993–1009 (2021).
- 588 11. C. Adaikkan, L.-H. Tsai, Gamma Entrainment: Impact on Neurocircuits, Glia, and Therapeutic
589 Opportunities. *Trends Neurosci.* **43**, 24–41 (2020).

- 590 12. C. Adaikkan, S. J. Middleton, A. Marco, P.-C. Pao, H. Mathys, D. N.-W. Kim, F. Gao, J. Z. Young,
591 H.-J. Suk, E. S. Boyden, T. J. McHugh, L.-H. Tsai, Gamma Entrainment Binds Higher-Order Brain
592 Regions and Offers Neuroprotection. *Neuron* **102**, 929-943.e8 (2019).
- 593 13. H. F. Iaccarino, A. C. Singer, A. J. Martorell, A. Rudenko, F. Gao, T. Z. Gillingham, H. Mathys, J.
594 Seo, O. Kritskiy, F. Abdurrob, C. Adaikkan, R. G. Canter, R. Rueda, E. N. Brown, E. S. Boyden, L.-H.
595 Tsai, Gamma frequency entrainment attenuates amyloid load and modifies microglia. *Nature* **540**, 230–
596 235 (2016).
- 597 14. A. J. Martorell, A. L. Paulson, H.-J. Suk, F. Abdurrob, G. T. Drummond, W. Guan, J. Z. Young, D.
598 N.-W. Kim, O. Kritskiy, S. J. Barker, V. Mangena, S. M. Prince, E. N. Brown, K. Chung, E. S. Boyden,
599 A. C. Singer, L.-H. Tsai, Multi-sensory Gamma Stimulation Ameliorates Alzheimer’s-Associated
600 Pathology and Improves Cognition. *Cell* **177**, 256-271.e22 (2019).
- 601 15. H.-J. Suk, N. Buie, G. Xu, A. Banerjee, E. S. Boyden, L.-H. Tsai, Vibrotactile stimulation at gamma
602 frequency mitigates pathology related to neurodegeneration and improves motor function. *Front. Aging*
603 *Neurosci.* **15** (2023).
- 604 16. K. M. Garza, L. Zhang, B. Borron, L. B. Wood, A. C. Singer, Gamma visual stimulation induces a
605 neuroimmune signaling profile distinct from acute neuroinflammation. *J. Neurosci.* **40**, 1211–1225
606 (2020).
- 607 17. L. Zheng, M. Yu, R. Lin, Y. Wang, Z. Zhuo, N. Cheng, M. Wang, Y. Tang, L. Wang, S.-T. Hou,
608 Rhythmic light flicker rescues hippocampal low gamma and protects ischemic neurons by enhancing
609 presynaptic plasticity. *Nat. Commun.* **11**, 3012 (2020).
- 610 18. A. Cimenser, E. Hempel, T. Travers, N. Strozewski, K. Martin, Z. Malchano, M. Hajós, Sensory-
611 Evoked 40-Hz Gamma Oscillation Improves Sleep and Daily Living Activities in Alzheimer’s Disease
612 Patients. *Front. Syst. Neurosci.* **15** (2021).
- 613 19. Q. He, K. M. Colon-Motas, A. F. Pybus, L. Piendel, J. K. Seppa, M. L. Walker, C. M. Manzanares, D.
614 Qiu, S. Miocinovic, L. B. Wood, A. I. Levey, J. J. Lah, A. C. Singer, A feasibility trial of gamma sensory
615 flicker for patients with prodromal Alzheimer’s disease. *Alzheimers Dement. Transl. Res. Clin. Interv.* **7**,
616 e12178 (2021).
- 617 20. D. Chan, H.-J. Suk, B. L. Jackson, N. P. Milman, D. Stark, E. B. Klerman, E. Kitchener, V. S. F.
618 Avalos, G. de Weck, A. Banerjee, S. D. Beach, J. Blanchard, C. Stearns, A. D. Boes, B. Uitermarkt, P.
619 Gander, M. H. Iii, E. J. Sternberg, A. Nieto-Castanon, S. Anteraper, S. Whitfield-Gabrieli, E. N. Brown,
620 E. S. Boyden, B. C. Dickerson, L.-H. Tsai, Gamma frequency sensory stimulation in mild probable
621 Alzheimer’s dementia patients: Results of feasibility and pilot studies. *PLOS ONE* **17**, e0278412 (2022).
- 622 21. L. P. Rybak, D. Mukherjea, S. Jajoo, V. Ramkumar, Cisplatin Ototoxicity and Protection: Clinical and
623 Experimental Studies. *Tohoku J. Exp. Med.* **219**, 177–186 (2009).
- 624 22. Y. Li, Y. Li, J. Li, G. Pi, W. Tan, Paclitaxel- and/or cisplatin-induced ocular neurotoxicity: a case
625 report and literature review. *OncoTargets Ther.* **7**, 1361–1366 (2014).

- 626 23. H. Takeuchi, Y. Taki, Y. Sassa, H. Hashizume, A. Sekiguchi, A. Fukushima, R. Kawashima, Brain
627 structures associated with executive functions during everyday events in a non-clinical sample. *Brain*
628 *Struct. Funct.* **218**, 1017–1032 (2013).
- 629 24. C. Bagnall-Moreau, S. Chaudhry, K. Salas-Ramirez, T. Ahles, K. Hubbard, Chemotherapy induced
630 cognitive impairment is associated with increased inflammation and oxidative damage in the
631 hippocampus. *Mol. Neurobiol.* **56**, 7159–7172 (2019).
- 632 25. M. J. Sekeres, M. Bradley-Garcia, A. Martinez-Canabal, G. Winocur, Chemotherapy-Induced
633 Cognitive Impairment and Hippocampal Neurogenesis: A Review of Physiological Mechanisms and
634 Interventions. *Int. J. Mol. Sci.* **22**, 12697 (2021).
- 635 26. X. Huo, T. M. Reyes, C. J. Heijnen, A. Kavelaars, Cisplatin treatment induces attention deficits and
636 impairs synaptic integrity in the prefrontal cortex in mice. *Sci. Rep.* **8**, 17400 (2018).
- 637 27. N. Meyer, J. E. Rinholm, Mitochondria in Myelinating Oligodendrocytes: Slow and Out of Breath?
638 *Metabolites* **11**, 359 (2021).
- 639 28. A. Grubman, X. Y. Choo, G. Chew, J. F. Ouyang, G. Sun, N. P. Croft, F. J. Rossello, R. Simmons, S.
640 Buckberry, D. V. Landin, J. Pflueger, T. H. Vandekolk, Z. Abay, Y. Zhou, X. Liu, J. Chen, M. Larcombe,
641 J. M. Haynes, C. McLean, S. Williams, S. Y. Chai, T. Wilson, R. Lister, C. W. Pouton, A. W. Purcell, O.
642 J. L. Rackham, E. Petretto, J. M. Polo, Transcriptional signature in microglia associated with A β plaque
643 phagocytosis. *Nat. Commun.* **12**, 3015 (2021).
- 644 29. D. R. Green, T. H. Oguin, J. Martinez, The clearance of dying cells: table for two. *Cell Death Differ.*
645 **23**, 915–926 (2016).
- 646 30. J. Han, M. Wang, M. Ren, H. Lou, Contributions of triggering-receptor-expressed-on-myeloid-cells-2
647 to neurological diseases. *Int. J. Neurosci.* **127**, 368–375 (2017).
- 648 31. S. Safaiyan, S. Besson-Girard, T. Kaya, L. Cantuti-Castelvetri, L. Liu, H. Ji, M. Schifferer, G. Gouna,
649 F. Usifo, N. Kannaiyan, D. Fitzner, X. Xiang, M. J. Rossner, M. Brendel, O. Gokce, M. Simons, White
650 matter aging drives microglial diversity. *Neuron* **109**, 1100-1117.e10 (2021).
- 651 32. L. Cantuti-Castelvetri, D. Fitzner, M. Bosch-Queralt, M.-T. Weil, M. Su, P. Sen, T. Ruhwedel, M.
652 Mitkovski, G. Trendelenburg, D. Lütjohann, W. Möbius, M. Simons, Defective cholesterol clearance
653 limits remyelination in the aged central nervous system. *Science* **359**, 684–688 (2018).
- 654 33. J. C. Dugas, A. Ibrahim, B. A. Barres, The T3-induced gene KLF9 regulates oligodendrocyte
655 differentiation and myelin regeneration. *Mol. Cell. Neurosci.* **50**, 45–57 (2012).
- 656 34. K. Shen, M. Reichelt, R. V. Kyauk, H. Ngu, Y.-A. A. Shen, O. Foreman, Z. Modrusan, B. A.
657 Friedman, M. Sheng, T. J. Yuen, Multiple sclerosis risk gene Mertk is required for microglial activation
658 and subsequent remyelination. *Cell Rep.* **34**, 108835 (2021).
- 659 35. M. Leo, L.-I. Schmitt, M. Erkel, M. Melnikova, J. Thomale, T. Hagenacker, Cisplatin-induced
660 neuropathic pain is mediated by upregulation of N-type voltage-gated calcium channels in dorsal root
661 ganglion neurons. *Exp. Neurol.* **288**, 62–74 (2017).

- 662 36. N. M.-B. Ben Abdallah, J. Fuss, M. Trusel, M. J. Galsworthy, K. Bobsin, G. Colacicco, R. M. J.
663 Deacon, M. A. Riva, C. Kellendonk, R. Sprengel, H.-P. Lipp, P. Gass, The puzzle box as a simple and
664 efficient behavioral test for exploring impairments of general cognition and executive functions in mouse
665 models of schizophrenia. *Exp. Neurol.* **227**, 42–52 (2011).
- 666 37. J. H. Schornagel, J. G. McVie, The clinical pharmacology of methotrexate. *Cancer Treat. Rev.* **10**,
667 53–75 (1983).
- 668 38. J. M. Williamson, D. A. Lyons, Myelin Dynamics Throughout Life: An Ever-Changing Landscape?
669 *Front. Cell. Neurosci.* **12** (2018).
- 670 39. S. A. Neely, J. M. Williamson, A. Klingseisen, L. Zoupi, J. J. Early, A. Williams, D. A. Lyons, New
671 oligodendrocytes exhibit more abundant and accurate myelin regeneration than those that survive
672 demyelination. *Nat. Neurosci.* **25**, 415–420 (2022).
- 673 40. J. F. Alexander, A. V. Seua, L. D. Arroyo, P. R. Ray, A. Wangzhou, L. Heiß-Lückemann, M.
674 Schedlowski, T. J. Price, A. Kavelaars, C. J. Heijnen, Nasal administration of mitochondria reverses
675 chemotherapy-induced cognitive deficits. *Theranostics* **11**, 3109–3130 (2021).
- 676 41. G. Winocur, M. A. Binns, I. Tannock, Donepezil reduces cognitive impairment associated with anti-
677 cancer drugs in a mouse model. *Neuropharmacology* **61**, 1222–1228 (2011).
- 678 42. M. A. Fuertes, J. Castilla, C. Alonso, J. M. Pérez, Cisplatin biochemical mechanism of action: from
679 cytotoxicity to induction of cell death through interconnections between apoptotic and necrotic pathways.
680 *Curr. Med. Chem.* **10**, 257–266 (2003).
- 681 43. B. N. Cronstein, T. M. Aune, Methotrexate and its mechanisms of action in inflammatory arthritis.
682 *Nat. Rev. Rheumatol.* **16**, 145–154 (2020).
- 683 44. M. Cheng, L. Yang, Z. Dong, M. Wang, Y. Sun, H. Liu, X. Wang, N. Sai, G. Huang, X. Zhang, Folic
684 acid deficiency enhanced microglial immune response via the Notch1/nuclear factor kappa B p65
685 pathway in hippocampus following rat brain I/R injury and BV2 cells. *J. Cell. Mol. Med.* **23**, 4795–4807
686 (2019).
- 687 45. M. Dhaynaut, G. Sprugnoli, D. Cappon, J. Macone, J. S. Sanchez, M. D. Normandin, N. J. Guehl, G.
688 Koch, R. Paciorek, A. Connor, D. Press, K. Johnson, A. Pascual-Leone, G. El Fakhri, E. Santarnecchi,
689 Impact of 40Hz Transcranial Alternating Current Stimulation on Cerebral Tau Burden in Patients with
690 Alzheimer’s Disease: A Case Series. *J. Alzheimers Dis. JAD* **85**, 1667–1676 (2022).
- 691 46. S. L. Wolock, R. Lopez, A. M. Klein, Scrublet: Computational Identification of Cell Doublets in
692 Single-Cell Transcriptomic Data. *Cell Systems* **8**, 281-291.e9 (2019).
- 693 47. F. A. Wolf, P. Angerer, F. J. Theis, SCANPY: large-scale single-cell gene expression data analysis.
694 *Genome Biology* **19**, 15 (2018).
- 695 48. W. E. Johnson, C. Li, A. Rabinovic, Adjusting batch effects in microarray expression data using
696 empirical Bayes methods. *Biostatistics* **8**, 118–127 (2007).

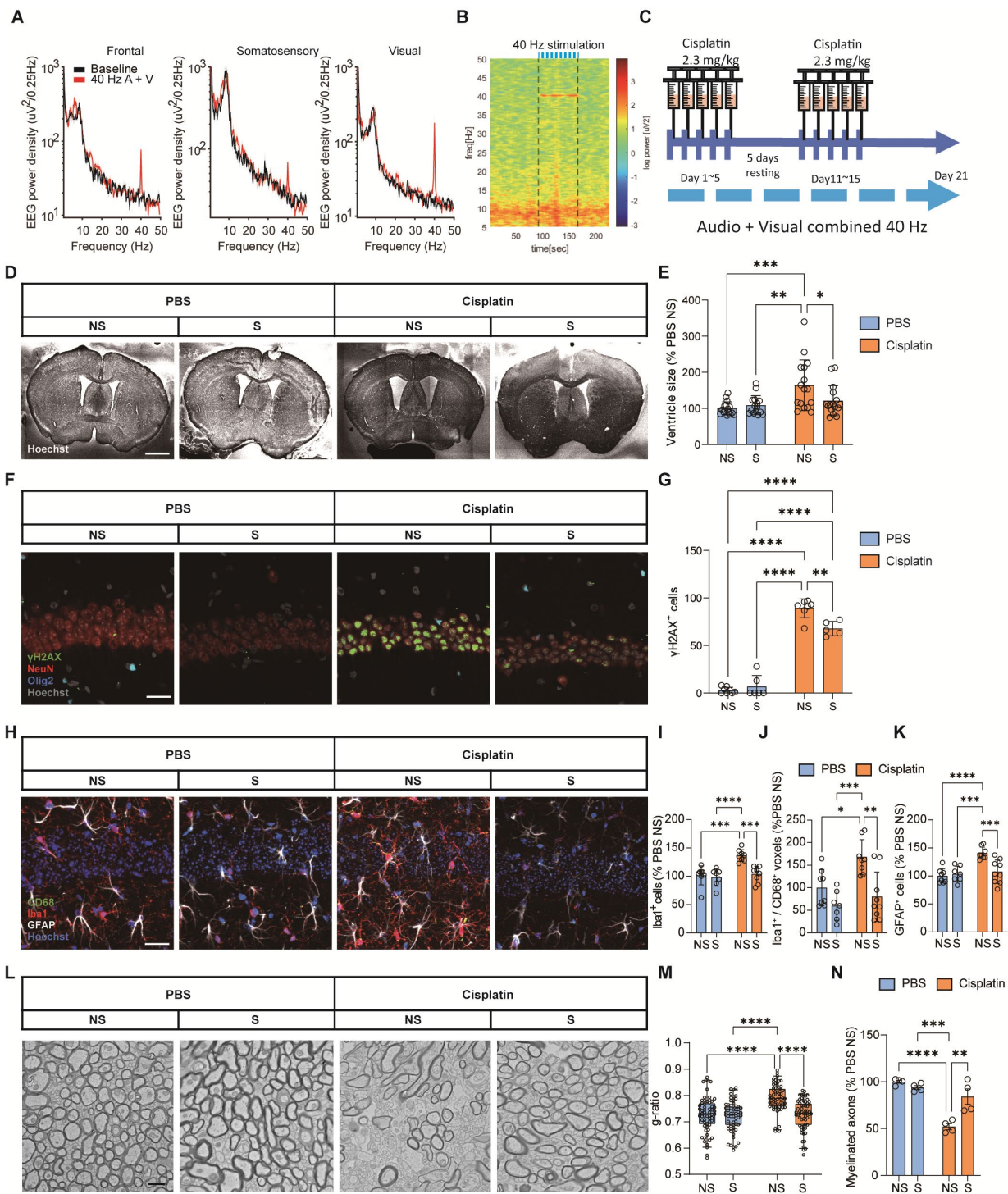
697 49. I. Korsunsky, N. Millard, J. Fan, K. Slowikowski, F. Zhang, K. Wei, Y. Baglaenko, M. Brenner, P.
698 Loh, S. Raychaudhuri, Fast, sensitive and accurate integration of single-cell data with Harmony. *Nat*
699 *Methods* **16**, 1289–1296 (2019).

700 50. K. Polański, M. D. Young, Z. Miao, K. B. Meyer, S. A. Teichmann, J.-E. Park, BBKNN: fast batch
701 alignment of single cell transcriptomes. *Bioinformatics* **36**, 964–965 (2020).

702 51. V. A. Traag, L. Waltman, N. J. van Eck, From Louvain to Leiden: guaranteeing well-connected
703 communities. *Sci Rep* **9**, 5233 (2019).

704

705



706

707

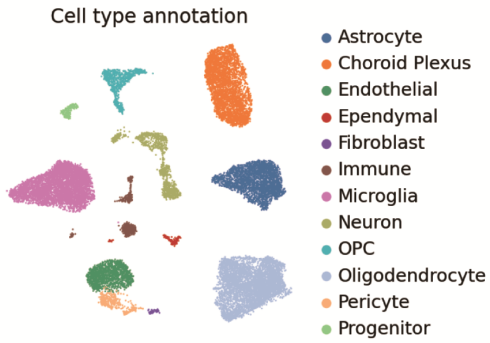
708

709 **Fig. 1. GENUS ameliorates chemobrain pathology.**

710 (A) EEG power density measured (n = 4 animals per group). (B) Representative spectrogram
711 from visual cortex. (C) Experimental design. (D) Tile scan of whole brain slice stained with
712 Hoechst. Scale bar: 1 mm. (E) Mean ventricle size per group.. (F) γ H2AX, NeuN, Olig2, and
713 Hoechst staining of hippocampal CA1 area. Scale bar: 25 μ m. (G) Mean number of γ H2AX⁺
714 cells per image. (H) CD68, Iba1, GFAP, Hoechst staining of hippocampal CA1 area. Scale bar:
715 25 μ m. (I) Mean number of Iba1⁺ cells per region of interest (ROI). (J) Mean volume of Iba1⁺
716 CD68⁺ signal in ROI. (K) Mean number of GFAP⁺ cells per ROI. (L) TEM images of corpus
717 callosum. Scale bar: 1 μ m. (M) Box plot (mean + 5-95%) of g-ratio. (N) Mean number of
718 myelinated axons. Data are mean \pm SD. Two-way ANOVA, Tukey's multiple comparison test.

719

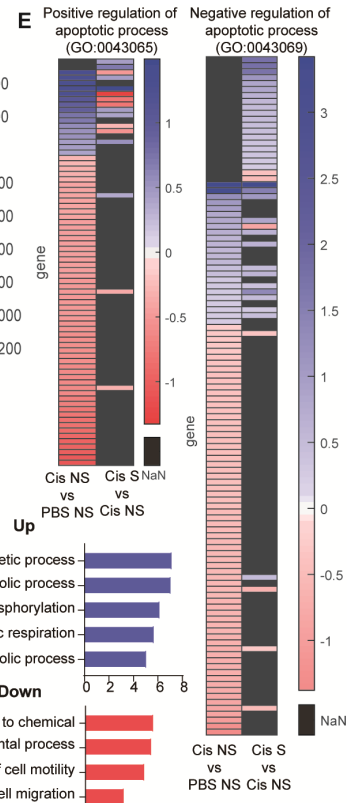
A



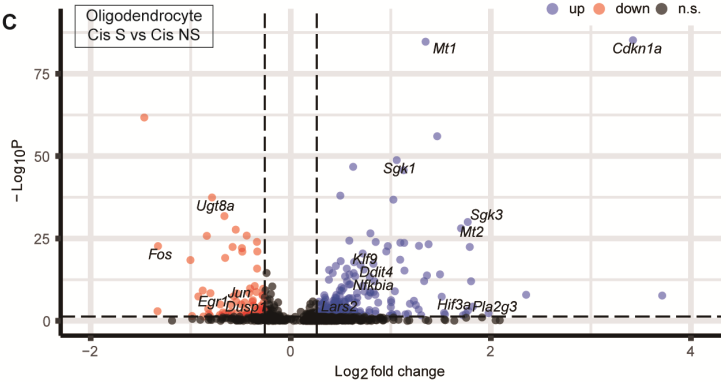
B

Celltype	Cis NS vs PBS NS		Cis S vs Cis NS	
	Up	Down	Up	Down
Oligodendrocyte	272	1313	321	112
Microglia	416	411	42	41
Choroid plexus	310	240	44	25
Astrocyte	122	258	49	50
Neuron	66	146	8	12
OPC	35	78	4	1
Endothelial	126	58	67	12
Pericyte	0	12	2	1
Ependymal	5	5	0	0
Immune	19	5	0	0
Progenitor	4	3	0	0

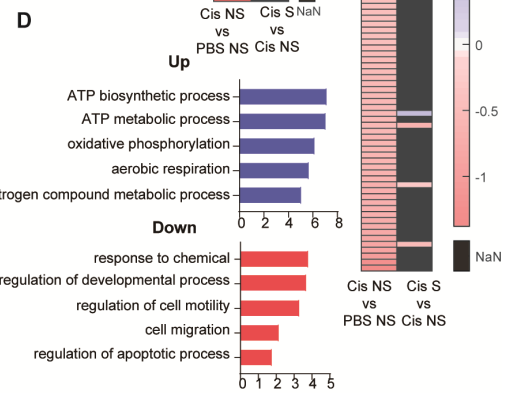
E



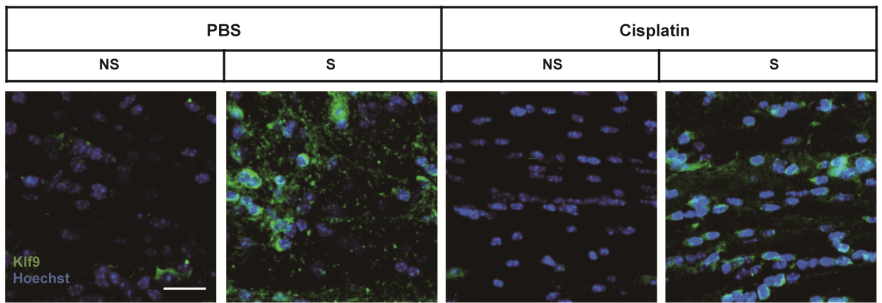
C



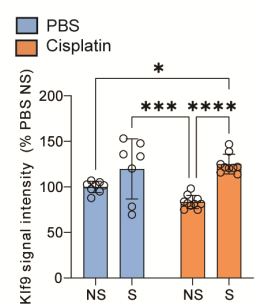
D



F



G



720

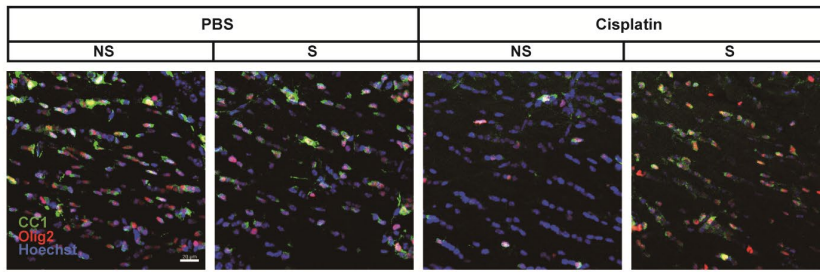
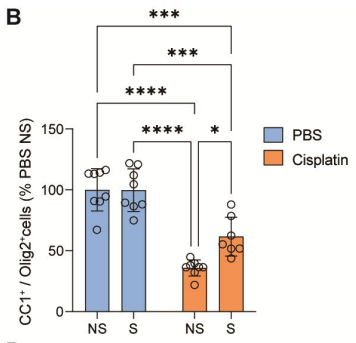
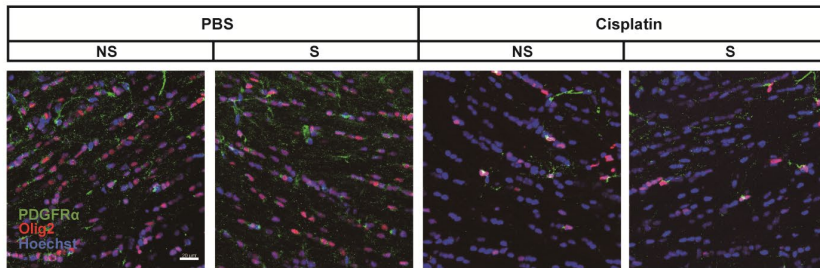
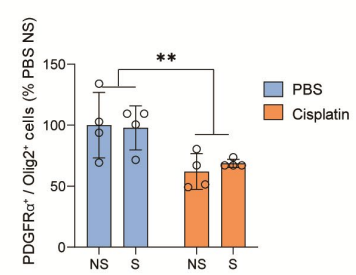
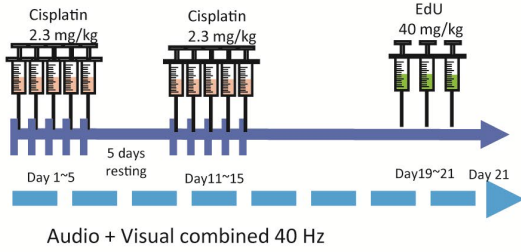
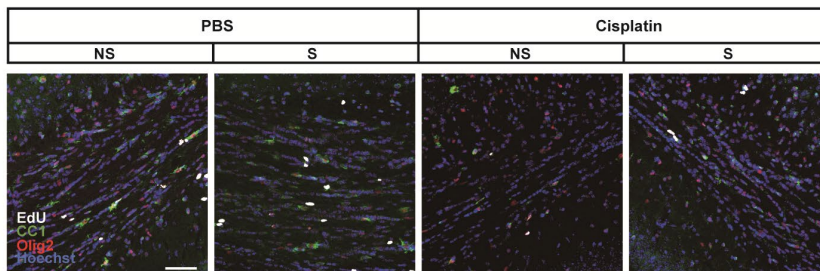
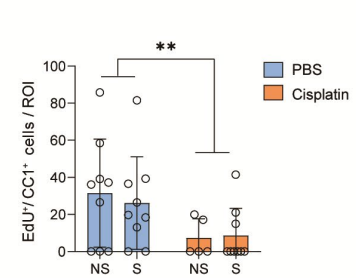
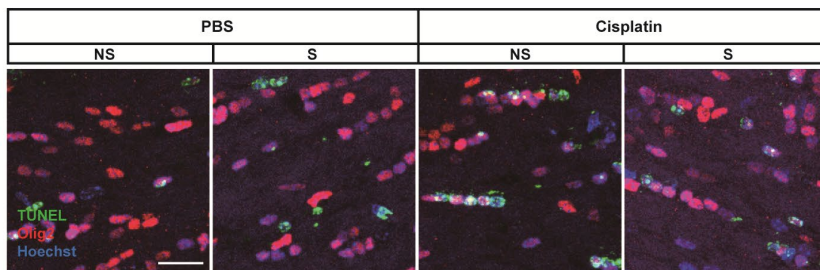
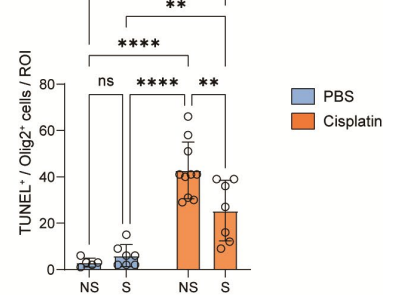
721

722

723 **Fig. 2. scRNA-seq reveals an altered transcriptome in oligodendrocytes.**

724 (A) UMAP showing sequenced single cells clustered into each cell type. (B) Number of DEG
725 across cell types between Cis NS vs. PBS NS and Cis S vs. Cis NS. (C) Volcano plot showing
726 DEG between Cis NS and PBS NS oligodendrocyte. (D) Upregulated and downregulated GO
727 terms in Cis S vs. Cis NS oligodendrocyte. (E) Upregulated and downregulated) DEG in GO terms
728 “Positive regulation of apoptotic process” and “Negative regulation of apoptotic process” in Cis
729 NS vs. PBS NS and Cis S vs. Cis NS oligodendrocytes. (F) Klf9 and Hoechst staining of corpus
730 callosum area. Scale bar: 20 μm . (G) Mean signal intensity of Klf9 staining. Data are mean \pm SD.
731 Two-way ANOVA, Tukey’s multiple comparison test.

732

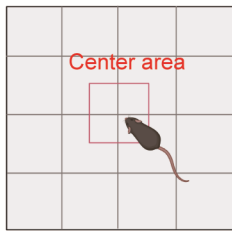
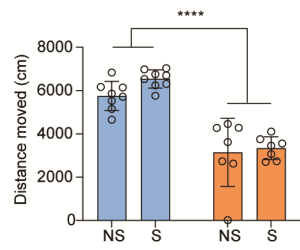
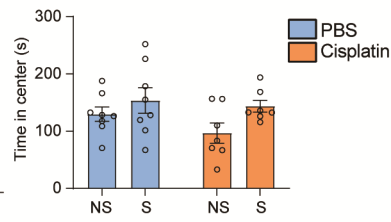
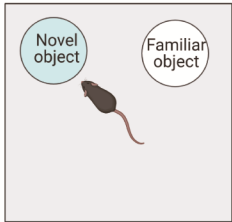
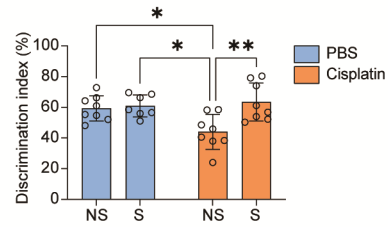
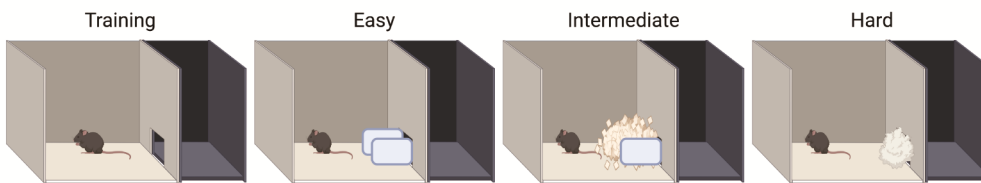
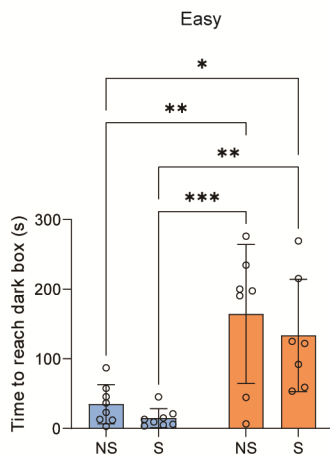
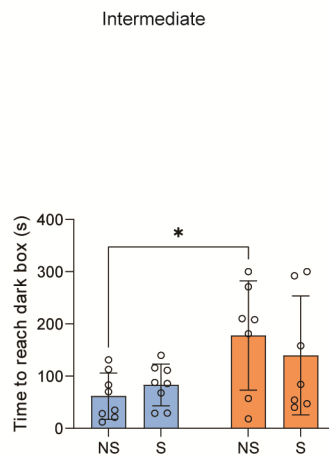
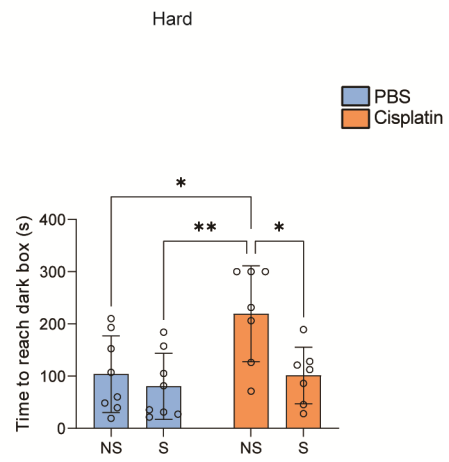
A**B****C****D****E****F****G****H****I**

734

735 **Fig. 3. GENUS promotes oligodendrocyte survival from cisplatin treatment.**

736 (A) CC1 , Olig2 and Hoechst staining of corpus callosum area. Scale bar: 20 μm . (B) Mean
737 number of oligodendrocytes ($\text{CC1}^+ \text{Olig2}^+$) per mm^2 . (C) PDGFR α , Olig2 and Hoechst staining of
738 corpus callosum area. Scale bar: 20 μm . (D) Mean number of OPC (PDGFR $\alpha^+ \text{Olig2}^+$) per mm^2 .
739 (E) Experimental scheme. (F) Edu, CC1, Olig2 and Hoechst staining of corpus callosum area.
740 Scale bar: 50 μm . (G) Mean number of newly formed oligodendrocytes ($\text{CC1}^+ \text{Olig2}^+ \text{EdU}^+$) per
741 mm^2 . (H) TUNEL, Olig2 and Hoechst staining of corpus callosum area. Scale bar: 25 μm . (I)
742 Mean number of apoptotic Olig2 $^+$ cells (TUNEL $^+$) per mm^2 Data are mean \pm SD. Two-way
743 ANOVA, Tukey's multiple comparison test.

744

A**B****C****D****E****F****G****H****I**

745

746

747

748 **Fig. 4. GENUS improves cognitive function in chemobrain animals.**

749 (A) Schematic drawing of OFT. (B) Mean value of total distance moved during 10 min OFT. (C)
750 Mean value of time spent in the center area during OFT. (D) Schematic drawing of NOR test. (E)
751 Mean value of discrimination index. One animal from PBS S group was excluded as it did not
752 spend more than 10 sec on exploring both objects. (F) Schematics of puzzle box test with different
753 obstacle settings. Animals must go through obstacles blocking the door to the dark chamber. (G-
754 I) Average of time to reach dark box during puzzle box test. (G) Average of three trials of easy
755 task. (H) Average of three trials of intermediate task. (I) Average of two trials of hard task. Data
756 are mean \pm SD. Two-way ANOVA, Tukey's multiple comparison test. Cartoon images were
757 created with Biorender.com.

758

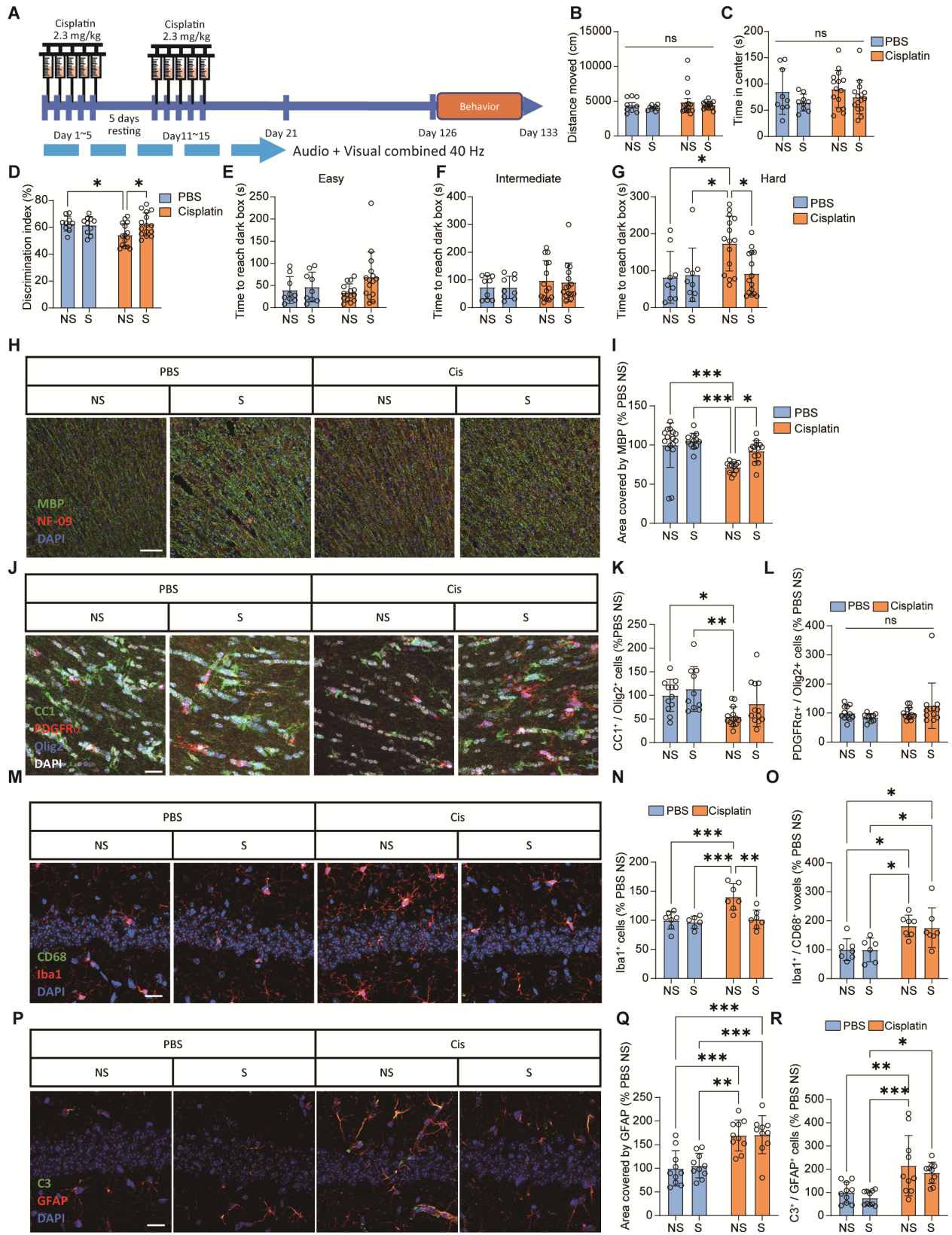
Timing of GENUS treatment	day 1 ~ 21 (27)		day 1 ~ 21		day 105 ~ 133	
Timing of behavior analysis	day 21 ~ 27		day 126 ~ 131		day 126 ~ 131	
Timing of sacrifice and tissue collection	day 21 for IHC		day 133		day 133	
GENUS	-	+	-	+	-	+
Comparison with PBS NS group						
Cognition						
NOR (discrimination index)	* ↓	↔	* ↓	↔	* ↓	* ↓
Puzzle box (Easy) (time to finish task)	** ↑	* ↑	↔	↔	↔	↔
Puzzle box (Intermediate) (time to finish task)	* ↑	↑	↔	↔	↔	↔
Puzzle box (Hard) (time to finish task)	* ↑	↔	* ↑	↔	* ↑	↔
Myelination						
Area covered by MBP	* ↓	↔	*** ↓	↔	* ↓	↓
Oligodendrocyte number	**** ↓	*** ↓	* ↓	↔	** ↓	** ↓
OPC number	** ↓	** ↓	↔	↔	↔	↔
Glial activation						
Iba1+ cells (CA1)	*** ↑	↔	*** ↑	↔	** ↑	** ↑
CD68/Iba1 voxels (CA1)	* ↑	↔	* ↑	* ↑	**** ↑	↔
Iba1+ voxels (corpus callosum)	** ↑	↔	** ↑	↔	* ↑	↔
CD68/Iba1 voxels (corpus callosum)	** ↑	↔	**** ↑	**** ↑	** ↑	↔
Area covered by GFAP	**** ↑	↔	*** ↑	*** ↑	* ↑	* ↑
C3/GFAP cells	** ↑	↔	** ↑	* ↑	** ↑	** ↑
Synaptic markers						
VGAT (PFC)	↔	* ↑	** ↑	** ↑	** ↑	* ↑
vGlut1 (PFC)	↔	↔	* ↓	* ↓	** ↓	** ↓
VGAT (CA1)	↔	↔	**** ↑	**** ↑	* ↑	↔
vGlut1 (CA1)	↔	↔	** ↓	** ↓	** ↓	** ↓

■ Chemobrain pathology
■ Improved pathology

760 **Table 1. Effect of GENUS treatment on chemobrain pathology depending on the timepoint**
761 **of the treatment.**

762 Summarized table of the analysis on the effect of GENUS treatment when given to cisplatin-based
763 chemobrain mouse model with varying time point of treatment and measurement. Asterisks show
764 statistical significance compared to PBS NS group. Arrows point the direction of change in mean
765 value of each measurement compared to PBS NS group. Two arrows were used when Cis NS and
766 Cis S have the same direction of change compared to PBS NS, but Cis S has significantly reduced
767 amplitude of the change (oligodendrocyte number in 21 days cohort). Chemobrain pathology was
768 color-coded as red and improved pathology with GENUS treatment was colored blue. Data were
769 not color-coded if the difference between PBS NS was not significant or not a chemobrain
770 pathology at the time point.

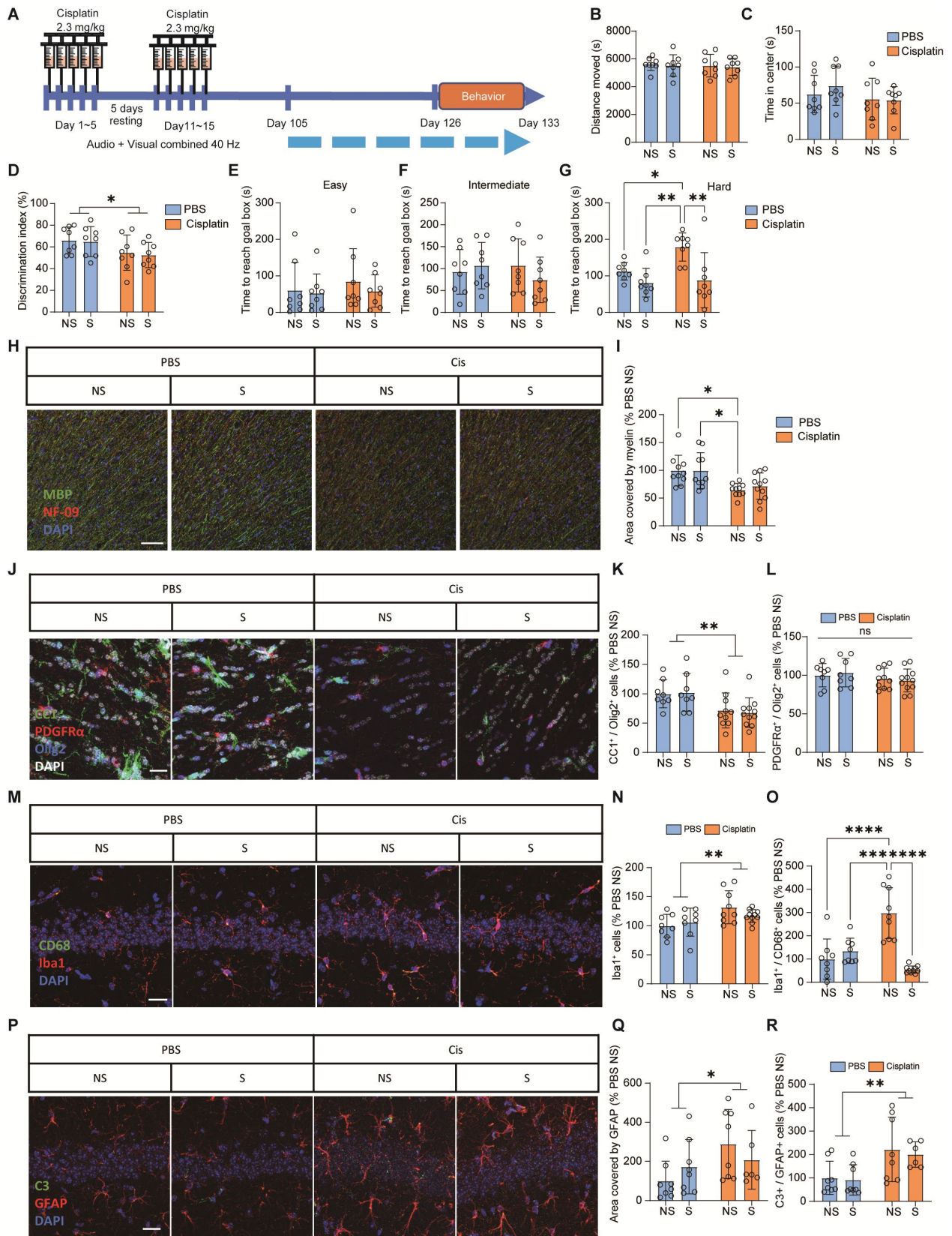
771



773 **Fig. 5. GENUS treatment during chemotherapy prevents progression of chemobrain**
774 **pathology.**

775 (A) Experimental design. (B) Mean value of total distance moved during 10 min OFT test. (C)
776 Mean value of time spent in center area during 10 min OFT test. (D) Mean value of discrimination
777 index during NOR test. (E-G) Average time spent to reach the goal box during three trials of puzzle
778 box test. (E) Average of three trials of easy task. (F) Average of three trials of intermediate task.
779 (G) Average of three trials of hard task. (H) MBP, NF-09 and DAPI staining of PFC area. Scale
780 bar: 50 μm (I) Mean value of area covered by MBP. (J) CC1, PDGFR α , Olig2 and DAPI staining
781 of corpus callosum area. Scale bar: 20 μm . (K) Number of CC1⁺ / Olig2⁺ cells. (L) Number of
782 PDGFR α ⁺ / Olig2⁺ cells. (M) CD68, Iba1 and DAPI staining of CA1 area. Scale bar: 20 μm . (N)
783 Mean value of Iba1⁺ voxels. (O) Mean value of CD68⁺ / Iba1⁺ voxels. (P) C3 (green), GFAP (red)
784 and DAPI (blue) staining of CA1 area. Scale bar: 20 μm . (Q) Mean value of area covered by GFAP.
785 (R) Mean value of C3⁺ / GFAP⁺. Data are mean \pm SD. Two-way ANOVA, Tukey's multiple
786 comparison test.

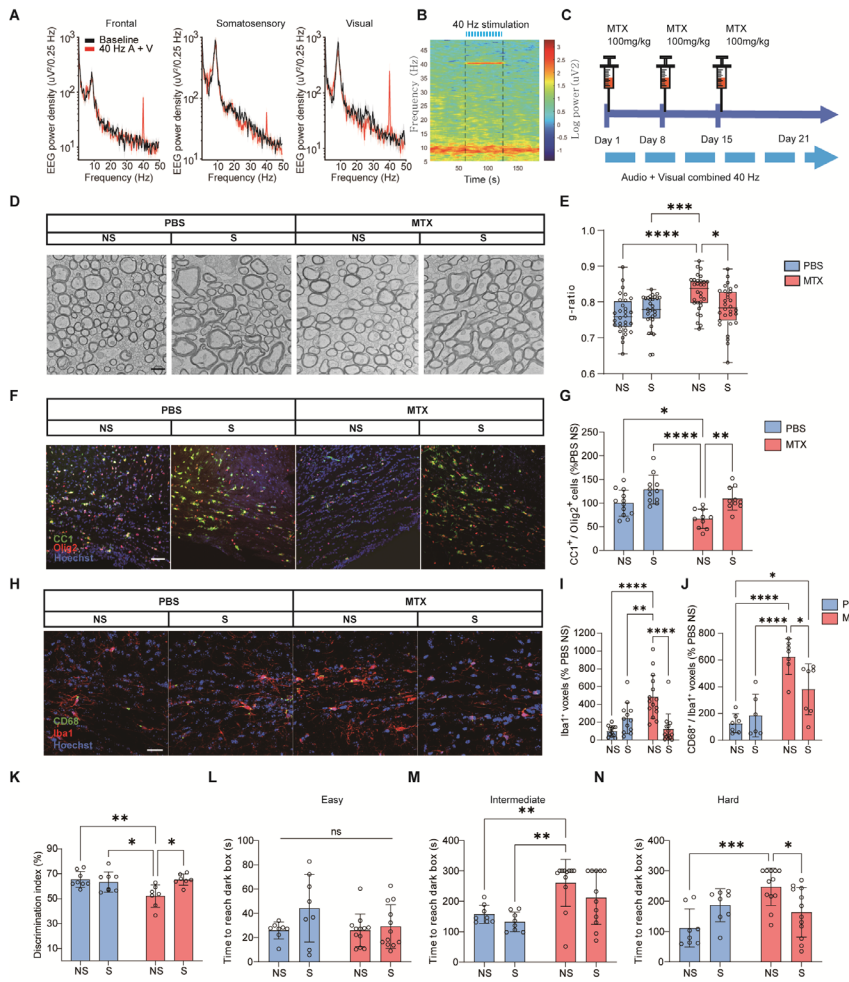
787



790 **Fig. 6. Post-chemotherapy GENUS treatment has limited effect on chemobrain pathology.**

791 (A) Experimental design to test if GENUS treatment post-chemotherapy can ameliorate
792 chemobrain pathology. (B) Mean value of total distance moved during 10 min OFT test. (C) Mean
793 value of time spent in center area during 10 min OFT test. (D) Mean value of discrimination index
794 during NOR test. (E-G) Average time spent to reach the goal box during three trials of puzzle box
795 test. (E) Average of three trials of easy task. (F) Average of three trials of intermediate task. (G)
796 Average of three trials of hard task. (H) MBP (green), NF-09 (red) and DAPI (blue) staining of
797 PFC area. Scale bar: 50 μm . (I) Mean value of area covered by MBP. (J) CC1 (green), PDGFR α
798 (red), Olig2 (blue) and DAPI (grey) staining of corpus callosum area. Scale bar: 20 μm . (K)
799 Number of CC1⁺ / Olig2⁺ cells. (L) Number of PDGFR α ⁺ / Olig2⁺ cells. (M) CD68 (green), Iba1
800 (red) and DAPI (blue) staining of CA1 area. Scale bar: 20 μm . (N) Mean value of Iba1⁺ voxels.
801 (O) Mean value of CD68⁺ / Iba1⁺ voxels. (P) C3 (green), GFAP (red) and DAPI (blue) staining of
802 CA1 area. Scale bar: 20 μm . (Q) Mean value of area covered by GFAP. (R) Mean value of C3⁺ /
803 GFAP⁺ cells. Data are mean \pm SD. Two-way ANOVA, Tukey's multiple comparison test.

804



805

806

807

808 **Fig. 7. GENUS ameliorates chemobrain pathology in the MTX-induced chemobrain mouse**
809 **model.**

810 (A) EEG power density measured at frontal, somatosensory and visual cortex screw (n = average
811 of 4 animals per group). (B) Representative spectrogram from visual cortex with and without 40
812 Hz auditory and visual stimulation. (C) Experimental design for MTX-induced chemobrain mouse
813 model and GENUS treatment. (D) TEM images of corpus callosum. Scale bar: 1 μm . (E) Box plot
814 (mean + 5-95%) of g-ratio. (F) CC1 (green), Olig2 (red) and Hoechst (blue) staining of corpus
815 callosum. Scale bar: 50 μm . (G) Mean value of number of oligodendrocytes (CC1⁺ Olig2⁺) per
816 mm^2 . (H) Iba1 (red) staining in corpus callosum. Scale bar: 20 μm . (I) Mean value of Iba1⁺ voxels
817 per mm^3 analyzed in 3D analysis software. (J) Mean value of CD68⁺ voxels per mm^3 analyzed in
818 3D analysis software. (K) Mean value of discrimination index during NOR. (L-N) Average time
819 to reach the dark box in puzzle box test. (L) Average of three trials of easy task. (M) Average of
820 three trials of intermediate task. (N) Average of two trials of hard task. Data are mean \pm SD. Two-
821 way ANOVA, Tukey's multiple comparison test.

822

823 **Materials and Methods**

824 **Animals.**

825 **Cisplatin-induced chemo brain model** 9-week-old C57/BL6J female mouse received intraperitoneal (i.p.)
826 injection of either 2.3 mg/kg cisplatin or volume-matched PBS for 5 consecutive days, had 5 days resting
827 period, and then received another 5 days of 2.3 mg/kg cisplatin or volume-matched PBS. Stim group
828 received 1 hr of 40 Hz audio + visual sensory stimulation immediately after the first injection (or 105 days
829 post injection depending on the experimental design), and then received 1 hr stimulation every day until
830 the day before they were sacrificed. No stim group stayed under a dim light for 1 hr immediately after the
831 first injection, and then stayed under a dim light for 1 hr every day until the day before they were sacrificed.
832 Every animal was single-caged in a cage covered with a black-plastic bag on every wall but one side for
833 the duration of 1 hr stim/sham period and then group housed with their littermates.

834 **MTX-induced chemo brain model** P21 C57/BL6J male mice received i.p. injection of either 100 mg/kg
835 MTX or volume-matched PBS on P21, P28, P35. Stim and no stim went through the same procedure as
836 described in cisplatin treated animals.

837 All animals were handled and sacrificed as approved by the Massachusetts Institute of Technology
838 Committee on Animal Care (MIT CAC).

839 **EEG recording** EEG recording screws were implanted in the skull at visual (Anteroposterior (AP): -2.95
840 mm, Mediolateral (ML): +1 mm), somatosensory (AP: -1.5 mm, ML: +1.5 mm) and prefrontal (AP: +2.3
841 mm, ML: +1 mm) cortex locations using a stereotaxic apparatus (Cisplatin n = 4; MTX n = 4). Reference
842 screw was implanted in the skull above cerebellum (AP: -7 mm, ML: 0 mm). All screws were secured to
843 the skull using dental acrylic. After surgery, animals were housed individually in ventilated cages, allowed
844 to recover from the surgery for two weeks and then started to receive cisplatin or MTX following the chemo

845 brain model induction protocol described above. On the 21st day from the first drug injection, animals were
846 transferred to separate custom-made Plexiglas cages (20.3 × 32 × 35 cm), which were placed in sound-
847 attenuated, electromagnetically shielded and light-controlled Faraday chambers (Med Associates Inc.), with
848 each chamber fitting two cages. EEG signals were recorded for 4 minutes during which 40 Hz auditory and
849 visual stimulation was presented for 60s. Data were acquired using a 96-channel Neurophysiology
850 Recording System (Tucker-Davis Technologies) and the recording software Synapse (Tucker-Davis
851 Technologies), and were saved on a local computer. The EEG signals were filtered between 0.1–100 Hz,
852 amplified (PZ5 NeuroDigitizer preamplifier, Tucker-Davis Technologies), and stored at a sampling rate of
853 305 Hz. The signals were then resampled at a sampling rate of 256 Hz using custom MATLAB code
854 (MathWorks, v2021). EEG recordings were partitioned into epochs of 4 s and epochs with recording
855 artifacts due to gross movements, chewing, or external electrostatic noise were not included in the
856 electrophysiological analysis. EEG power spectra were computed using a fast Fourier transform routine
857 (Hanning window) with a 0.25-Hz resolution and exported in the frequency range between 0 and 50 Hz for
858 spectral analysis.

859 **EdU labeling** 40mg/kg EdU (Thermo Fisher, A10044) was injected for 3 consecutive days according to
860 experimental schedule described in results section. Click-iT EdU Alexa Fluor 647 imaging kit (Thermo
861 Fisher, C10340) was used to stain brain sections according to manufacturer’s protocol.

862 **Behavior**

863 **Timeline**

864 For IHC and TEM analysis on Figs. 1, 3, figs. S2-4, animals received 2.3 mg/kg cisplatin or volume-
865 matched PBS on day 1-5, 11-15. GENUS treatment was given from day 1-21. Animals were sacrificed to
866 collect tissue on day 22. This cohort has been replicated two times.

867 For behavior tests on Fig. 4, animals received 2.3 mg/kg cisplatin or volume-matched PBS on day 1-5,
868 11-15. OFT was performed on day 21, NOR on day 23 and puzzle box test was performed from day
869 24~27. GENUS treatment was given from day 1-27. Animals were sacrificed on day 28. This cohort has
870 been replicated two times.

871 For behavior tests on Fig 5, animals received 2.3 mg/kg cisplatin or volume-matched PBS on day 1-5, 11-
872 15. GENUS treatment was given from day 1-21. OFT was performed on day 126, NOR on day 127 and
873 puzzle box test was performed on day 128~131. Animals were allowed to rest in their homecage for 2
874 days and then sacrificed on day 133 and samples were collected for IHC analysis. This cohort has been
875 replicated one time.

876 For behavior tests on Fig 6, animals received 2.3 mg/kg cisplatin or volume-matched PBS on day 1-5, 11-
877 15. OFT was performed on day 126, NOR on day 127 and puzzle box test was performed on day
878 128~131. GENUS treatment was given from day 105-132 and animals were sacrificed on day 133 and
879 samples were collected for IHC analysis. This cohort has been replicated one time.

880 For IHC analysis on Fig 7, animals received 100 mg/kg MTX or volume-matched PBS on day 1, 8, 15.
881 GENUS was given from day 1-21. Animals were sacrificed on day 22 to collect tissue samples. This
882 cohort has been replicated two times.

883 For behavior tests on Fig 7, animals received 100 mg/kg MTX or volume-matched PBS on day 1, 8, 15.
884 GENUS was given from day 1-21. OFT was performed on day 21, NOR on day 23 and puzzle box test
885 was performed from day 24~27. GENUS treatment was given from day 1-27. Animals were sacrificed on
886 day 28. This cohort has been replicated two times.

887 **OFT** Animals were placed in the center of 90 x 90 cm x 40 cm (W x L x H) white acryle box with
888 dividers (45 cm x 45 cm x 40 cm for single chamber) and their movement were tracked with a behavior

889 tracking software (EthoVision XT, noldus) for 10 min. 22.5 cm x 22.5 cm area in the center of the box
890 was marked as ‘center area’.

891 **Puzzle box test** Animals were placed in a testing arena containing a lighted (55 cm x 28 cm) and a dark
892 (15 cm x 28 cm) compartment with a connecting tunnel (4 cm x 4 cm x 2.5 cm), facing the farthest wall
893 from the dark compartment. 3 trials were performed for 3 days. 1 introductory period without any
894 obstacles blocking the tunnel and 2 ‘easy tasks’ in which animals have to pass a corridor (4 cm x 4 cm x
895 12 cm). On day 2, 1 ‘easy task’ and 2 ‘intermediate tasks’ in which the corridor is blocked with sawdust
896 and the animals have to dig through to reach the dark chamber were performed. On day 3, 1 ‘intermediate
897 task’ and 2 ‘hard tasks’ where the tunnel was plugged with a tissue were performed. Time of the first
898 entry to the dark chamber was recorded for every trial. If an animal failed to reach the dark chamber
899 within 5 min, the animal was removed from the apparatus and time to reach the dark chamber was marked
900 as 5 min.

901 **NOR** Animals were habituated in an OFT box for 10 min on 3 consecutive days. On the 4th day, two
902 identical wooden blocks (Premium wooden building blocks set, Cubbie Lee) were placed in the chamber,
903 and animals were allowed to explore the objects for 5 min, then the animals were returned to their
904 homecage for 5 min. In the test phase, one of the wooden block was switched to a novel wooden block
905 with a different shape, and the time spent exploring the familiar and new objects was measured for 10
906 min. Discrimination index was calculated as time spent to explore the new object divided by the sum of
907 time spent to explore both old and new object.

908 Discrimination index = $\frac{\text{Time spent to explore new object}}{\text{Time spent to explore new object} + \text{Time spent to explore familiar object}} \times 100 (\%)$

909 **Immunohistochemistry**

910 For the analysis of PFC, slices from anterior posterior (AP) +1.2 ~ 1.4 mm were selected. For the analysis
911 of corpus callosum, slices from AP +0.1 ~ -0.1 were selected and the corpus callosum area above lateral
912 ventricle was selected. For the measurement of corpus callosum thickness, three shortest lines connecting
913 the top and the bottom edge of corpus callosum was drawn 50 μm apart each and the average length of
914 line was calculated. For the analysis of CA1 and DG, slices from AP -1.7 ~ -1.8 were selected. Two slices
915 from each animal were analyzed and average value from the two slices was used as a single datapoint.
916 Each slice were selected with 200 μm interval.

917 20~40 μm thick vibratome sectioned brain slices were washed in PBS, then incubated in a blocking
918 solution (3 % normal donkey serum (Millipore Sigma, S30-M) and 0.3 % Triton X-100 (Sigma-Aldrich,
919 T8787-100ML) in PBS for 2 hrs. Then, slices were treated with a blocking solution containing α -CD68
920 (1:100, Abcam, ab12512), α -CC1 (1:20, Millipore, OP08), α -MBP (1:500, Millipore, AB9348), α -
921 γ H2AX (1:500, EMD Millipore, 05-636), α -Iba1 (1:500, SYSY, 234004), α -Olig2 (1:200, Abcam,
922 ab109186), α -GFAP (1:1000, Thermo Fisher, 130300), α -C3 (1:200, Abcam, ab11887), α -PDGFR α
923 (1:40, R&D systems, AF1062), α -Klf9 (1:100, antigen retrieval with pH 9 EDTA buffer, Thermo
924 scientific, PA5-112929), α -neurofilament medium (NF-09) (1:500, Abcam, ab7794), α -SOX2 (1:200,
925 R&D systems, AF2018), α -DCX (1:500, CST, 4604S) α -Ki67 (1:200, Invitrogen, 14-5698-82), α -vGlut1
926 (1:200, SYSY, 135 304) α -VGAT (1:200, SYSY, 131 003) in a 4 $^{\circ}\text{C}$ – 10 $^{\circ}\text{C}$ controlled cold room for 24
927 - 48 hours. Slices were washed with PBS, and then stained with α -rabbit IgG Alexa 488 conjugated
928 (1:500, Thermo Fisher, A-21206), α -rabbit IgG Alexa 555 conjugated (1:500, Thermo Fisher, A-27039),

929 α -mouse IgG Alexa 488 conjugated (1:500, Thermo Fisher, A-28175), α -chicken IgY Alexa 555
930 conjugated (1:500, Thermo Fisher A-21437) and α -chicken IgY Alexa 488 conjugated (1:500, Thermo
931 Fisher, A-11039) for 2 hrs at room temperature. Slices were washed with PBS and nuclei were stained
932 with Hoechst 33342 (1:500000, Thermo Fisher, H3570).

933 **Fluorescent *in situ* hybridization**

934 20 μ m brain slices was stained with RNAscope[®] multiplex kit (ACDbio, 320850, 320851) and probes for
935 *Cdkn1a* (ACDbio, 408551-C2) and *Mbp* (ACDbio, 451491-C3).

936 **TUNEL staining**

937 20 μ m brain slices was stained with Click-iT[™] Plus TUNEL Assay Kits for In Situ Apoptosis Detection
938 kit (Invitrogen, C10619) following manufacturer's protocol.

939 **Single cell RNA sequencing**

940 **Sample preparation** Animals were subjected to cisplatin and GENUS as described above and, on the
941 22nd day from the first cisplatin/GENUS treatment, they were anesthetized with isoflurane and cardiac
942 perfused with ice cold DPBS (Thermo Fisher Scientific, 14190235). A total of two cohorts of sequencing
943 samples were prepared. For one sequencing cohort, two hippocampus per animal were isolated and
944 homogenized using adult neural dissociation kit (Miltenyi bio, 130-092-628). For the second cohort, two
945 hippocampi per animal were isolated and four hippocampi from two animals were homogenized using an
946 adult neural tissue dissociation kit. The resulting single cell suspension was processed to generate a
947 cDNA library with targeted recovery of 5000 cells using 10x Genomics Chromium[™] Single Cell 3'
948 Library & Gel Bead Kit v3.1 (1000215, 1000268, 1000127). The library was sequenced on a NovaSeq
949 6000 (Illumina) using a NovaSeq S4 Flow Cell at the MIT bioinformatics core.

950 **scRNA-seq analysis**

951 Cells were called and aligned using the 10X CellRanger 5.0.0 pipeline. Next, using Scrublet(46), doublets
952 were called per-sample using default settings. Cell filtering was performed using the Scanpy(47) software
953 to the following quality control metrics: between 750 and 20000 total mRNA counts per cell, a Scrublet
954 score below 0.1, number of unique genes per cell above 500, percentage of counts in top 50 genes below
955 80%, and percentage of ribosomal protein genes below 25%. Next, normalization followed a standard
956 protocol of median-normalization and log1p transformation in Scanpy, followed by filtering to 5000
957 variable genes. To generate a UMAP embedding, ComBat(48), PCA, Harmony(49), and BBKNN(50)
958 were applied with default parameters to remove batch effect and to reduce dimensionality. Clusters were
959 computed using the Leiden(51) algorithm at default parameters. Cell types were assigned to Leiden
960 clusters by looking at marker genes between clusters by using the Wilcoxon rank-sum test between
961 clusters via the “rank_genes_groups” method in Scanpy with the “method” parameter set to “wilcoxon”.
962 Low quality cells were further removed via marker gene analysis, and the resulting UMAP and clusters
963 were re-generated using the aforementioned workflow.

964 DEG for each pair of conditions for each cell type were discovered by subsetting the data to contain only
965 the cell type of interest and pair of pathological conditions of interest, then running the
966 “rank_genes_groups” method in Scanpy with the “method” parameter set to “wilcoxon”.

967 GO analysis of DEG was implemented using the Logically Accelerated GO term finder (LAGO) tool with
968 the DEG cutoff of FDR < 0.05 and Log2FC > 0.26 (20% change). GO terms with more than 10 DEG
969 associated were selected.

970 **TEM imaging**

971 Animals were anesthetized with isoflurane and perfused with 1xPBS, followed by formaldehyde
972 glutaraldehyde 2.5% solution in sodium cacodylate buffer (EMS, 15949-1L). Brain tissues were sliced
973 into 1 mm thick slices and drop fixed in formaldehyde glutaraldehyde 2.5% solution in sodium cacodylate
974 buffer (EMS, 15949-1L).

975 TEM imaging of the corpus callosum area was performed by the Harvard Electron Microscope core.

976 **Data acquisition and statistical analysis**

977 OFT behavior was tracked with a behavior tracking software (EthoVision XT, Nodulus). NOR and puzzle
978 box behavior was scored by manual counting. Zeiss LSM 710, Zeiss LSM 880 and Zeiss LSM 900
979 confocal microscopes with Zen software were used to capture fluorescence images. A 3D image analysis
980 software (IMARIS, Bitplane) was used to score Iba1 and CD68 positive voxels, and the g-ratio, area
981 covered by fluorescent signal, ventricle size, and cell number counting was scored with ImageJ software.
982 Researchers were blinded for the experimental group during data analysis. All graphs are presented as
983 mean \pm SD

984

985

986

987

988

989

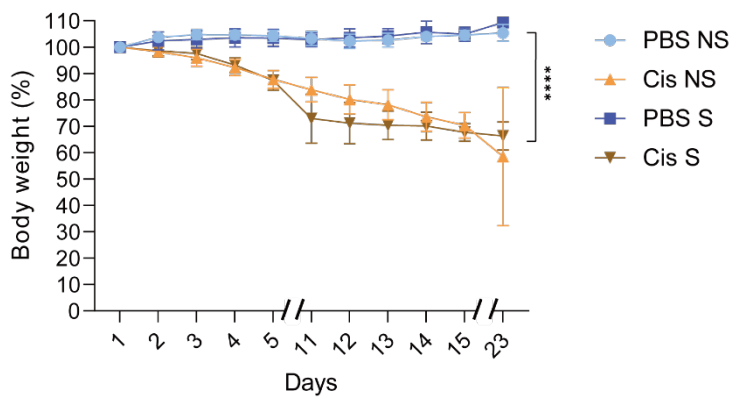
990

991

992

993

994

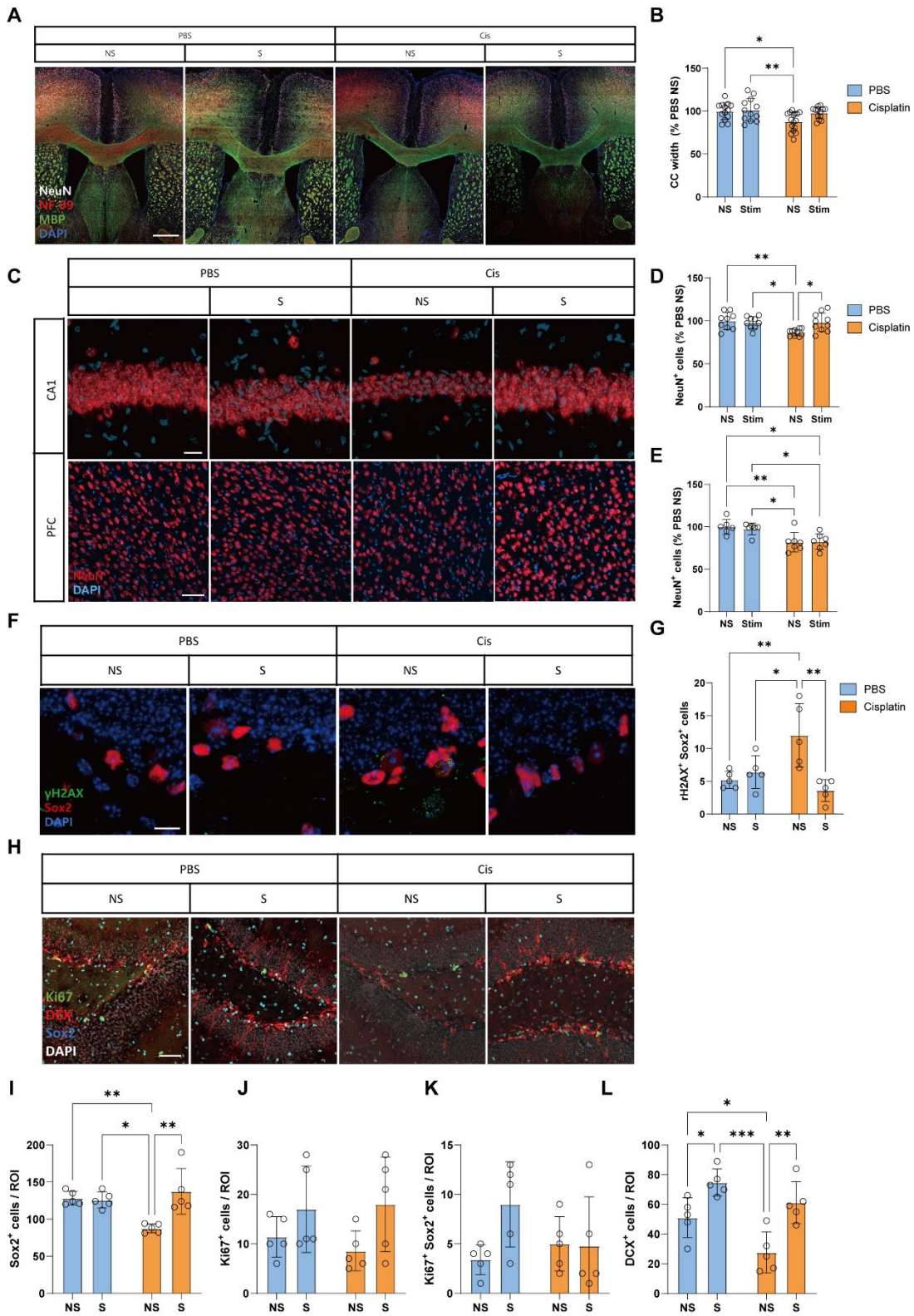


995

996 **fig. S1. Cisplatin reduces body weight with no effect from GENUS on body weight.**

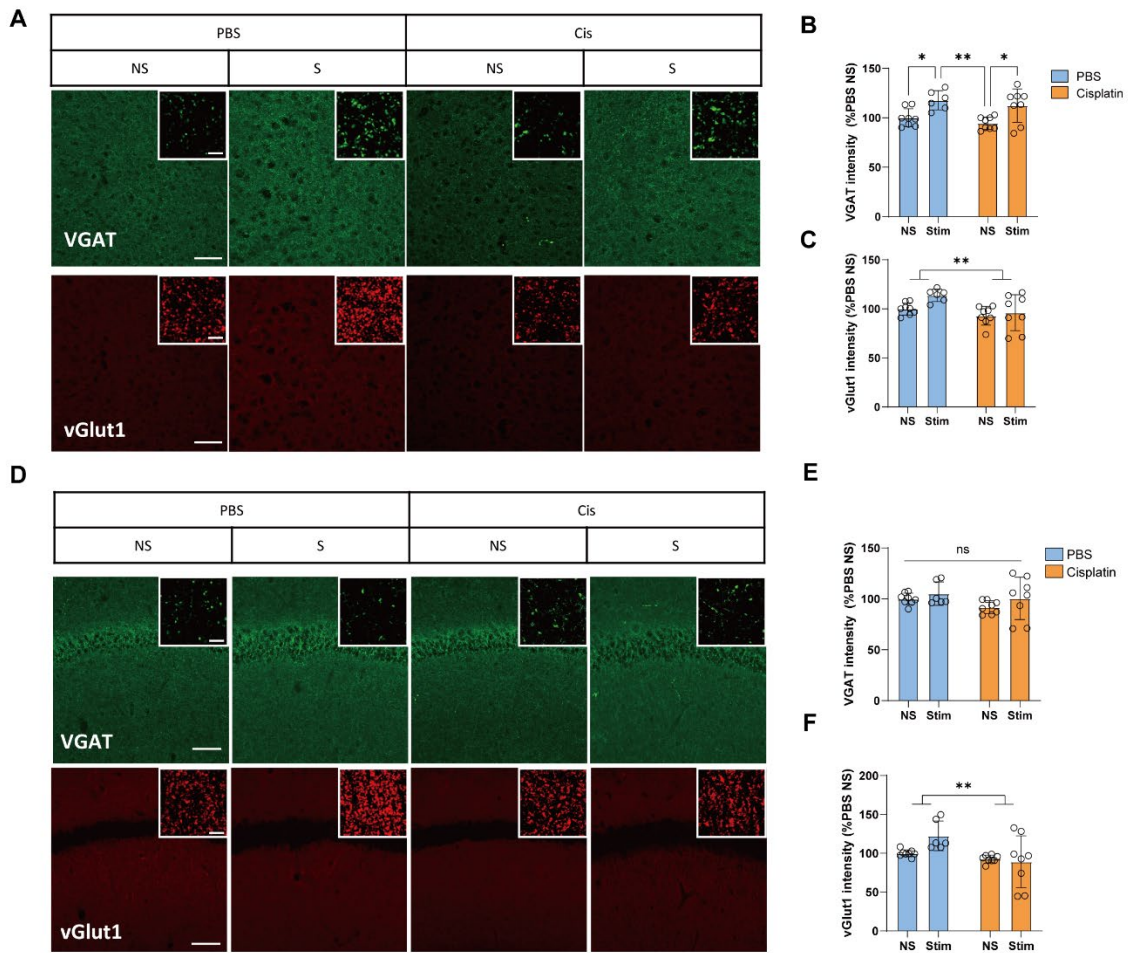
997 Body weight measured during cisplatin injection (PBS NS, n = 8; PBS S, n = 8; Cis NS, n = 7; Cis

998 S, n = 7, three-way ANOVA, effect of cisplatin ****P < 0.001)



1000 **fig. S2. GENUS reduces corpus callosum and neuronal lineage cell loss.**

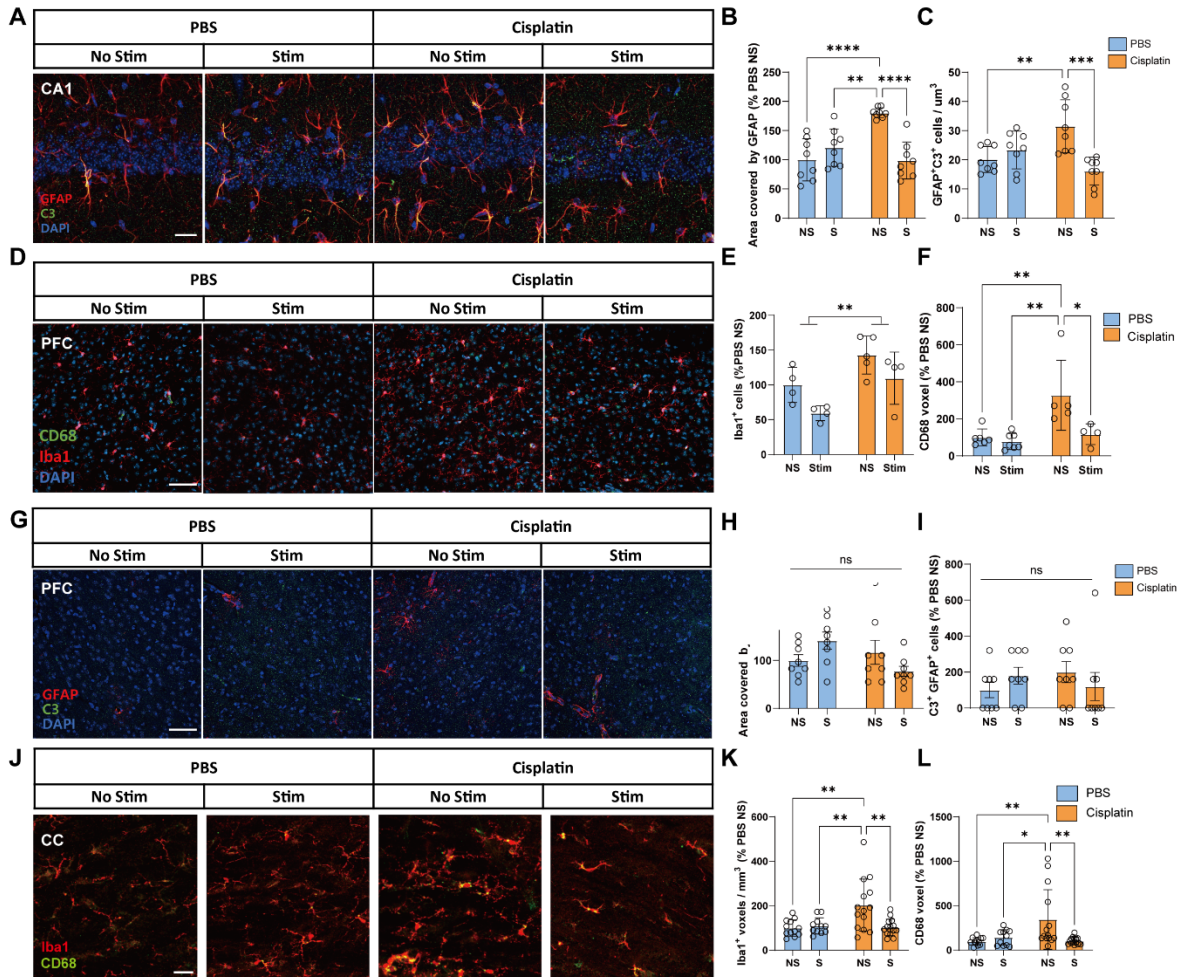
1001 (A) Staining of NeuN (grey), NF-09 (red), green (MBP) and DAPI (blue) of brain slices +1.0~0.9
1002 mm from bregma. The thickness of corpus callosum was measured on six-points marked on the
1003 image and averaged per animal. Scale bar: 500 μm . (B) Mean value of corpus callosum thickness
1004 (PBS NS, n = 13; PBS S, n = 12; Cis NS, n = 16; Cis S, n = 13, Two-way ANOVA, Tukey's
1005 multiple comparison test). (C) Staining of NeuN (red) and DAPI (blue) of PFC (top) and CA1
1006 (bottom) area. Scale bar: 50 μm (PFC), 20 μm (CA1). (D) Mean number of NeuN⁺ cells in the
1007 PFC area (PBS NS, n = 9; PBS S, n = 9; Cis NS, n = 10; Cis S, n = 10, Two-way ANOVA, Tukey's
1008 multiple comparison test). (E) Mean number of NeuN⁺ cells in the CA1 area (PBS NS, n = 6; PBS
1009 S, n = 6; Cis NS, n = 7; Cis S, n = 7, Two-way ANOVA, Tukey's multiple comparison test). (F)
1010 staining of γH2AX (green), Sox2 (red) and DAPI (blue) staining in the DG area. Scale bar: 10 μm .
1011 (G) Mean number of $\gamma\text{H2AX}^+ / \text{Sox2}^+$ cells in the DG area (PBS NS, n = 5; PBS S, n = 5; Cis NS,
1012 n = 5; Cis S, n = 5, Two-way ANOVA, Tukey's multiple comparison test). (H) Staining of Ki67
1013 (green), Dcx (red), Sox2 (blue) and DAPI (grey) of DG area. Scale bar: 50 μm . (I) Mean number
1014 of Sox2⁺ cells in the DG area (PBS NS, n = 5; PBS S, n = 5; Cis NS, n = 5; Cis S, n = 5, Two-way
1015 ANOVA, Tukey's multiple comparison test). (J) Mean number of Ki67⁺ cells in the DG area (PBS
1016 NS, n = 5; PBS S, n = 5; Cis NS, n = 5; Cis S, n = 5, Two-way ANOVA, Tukey's multiple
1017 comparison test). (K) Mean number of Ki67⁺ / Sox2⁺ cells in the DG area (PBS NS, n = 5; PBS S,
1018 n = 5; Cis NS, n = 5; Cis S, n = 5, Two-way ANOVA, Tukey's multiple comparison test). (L)
1019 Mean number of Dcx⁺ cells in the DG area (PBS NS, n = 5; PBS S, n = 5; Cis NS, n = 5; Cis S, n
1020 = 5, Two-way ANOVA, Tukey's multiple comparison test).



1022 **fig. S3 Inhibitory and excitatory synaptic markers at day 21.**

1023 (A) Staining of VGAT (green) and vGlut1 (red) of PFC area. Insert: 63x image of the PFC area.
1024 Scale bar: 50 μm (insert : 5 μm). (B) Mean value of VGAT signal intensity (PBS NS, n = 8; PBS
1025 S, n = 6; Cis NS, n = 8; Cis S, n = 8, Two-way ANOVA, Tukey's multiple comparison test). (C)
1026 Mean value of vGlut1 signal intensity (PBS NS, n = 8; PBS S, n = 6; Cis NS, n = 8; Cis S, n = 8,
1027 Two-way ANOVA, effect of cisplatin $**p < 0.01$). (D) Staining of VGAT (green) and vGlut1 (red)
1028 of CA1 area. Insert: 63x image of the CA1 area. Scale bar: 50 μm (insert : 5 μm). (E) Mean value
1029 of VGAT signal intensity (PBS NS, n = 8; PBS S, n = 6; Cis NS, n = 8; Cis S, n = 8, Two-way
1030 ANOVA, Tukey's multiple comparison test). (F) Mean value of vGlut1 signal intensity (PBS NS,
1031 n = 8; PBS S, n = 6; Cis NS, n = 8; Cis S, n = 8, Two-way ANOVA, effect of cisplatin $**p < 0.01$).

1032

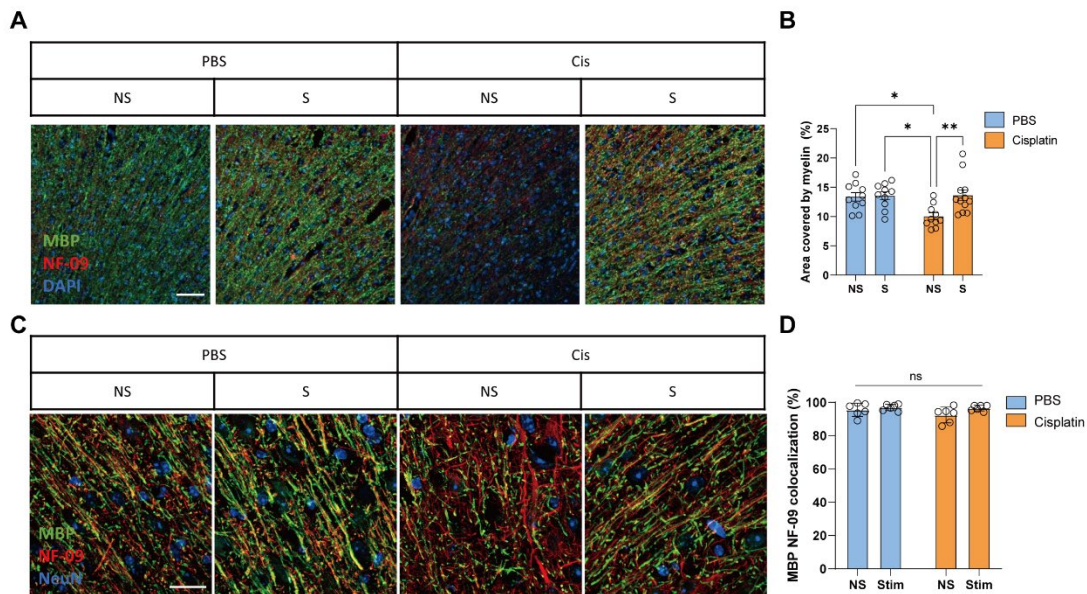


1034 **fig S4. GENUS reduces glial activation from cisplatin treatment.**

1035 (A) Staining of GFAP (red), C3 (green) and DAPI (blue) in CA1 area. Scale bar: 20 μm . (B) Mean
1036 value of area covered by GFAP⁺ (PBS NS, n = 8; PBS S, n = 8; Cis NS, n = 8; Cis S, n = 8, Two-
1037 way ANOVA, Tukey's multiple comparison test). (C) Mean number of GFAP⁺ / C3⁺ cells (PBS
1038 NS, n = 8; PBS S, n = 8; Cis NS, n = 8; Cis S, n = 8, Two-way ANOVA, Tukey's multiple
1039 comparison test). (D) Staining of CD68 (green), Iba1 (red) and DAPI (blue) of PFC area. Scale
1040 bar: 50 μm . (E) Mean value of Iba1⁺ voxels (PBS NS, n = 4; PBS S, n = 4; Cis NS, n = 5; Cis S,
1041 n = 4, Two-way ANOVA, Tukey's multiple comparison test). (F) Mean value of CD68⁺ / Iba1⁺
1042 voxels. (G) Staining of GFAP (red), C3 (green) and DAPI (blue) of PFC area. Scale bar: 50 μm .
1043 (H) Mean value of area covered by GFAP⁺ (PBS NS, n = 8; PBS S, n = 8; Cis NS, n = 8; Cis S, n
1044 = 8, Two-way ANOVA, Tukey's multiple comparison test). (I) Mean number of C3⁺ / GFAP⁺
1045 cells (PBS NS, n = 8; PBS S, n = 8; Cis NS, n = 8; Cis S, n = 8, Two-way ANOVA, Tukey's
1046 multiple comparison test). (J) Iba1 (red) and CD68 (green) staining of corpus callosum area. Scale
1047 bar: 20 μm . (K) Mean value of voxels of Iba1 signal per mm^3 measured in 3D analysis software
1048 (PBS NS, n = 12; PBS S, n = 11; Cis NS, n = 14; Cis S, n = 15, Two-way ANOVA, Tukey's
1049 multiple comparison test). (L) Mean value of voxels of CD68 signal overlapping with Iba1 signal
1050 per mm^3 measured in 3D analysis software (PBS NS, n = 12; PBS S, n = 9; Cis NS, n = 14; Cis S,
1051 n = 15, Two-way ANOVA, Tukey's multiple comparison test).

1052

1053



1054

1055 **fig S5. GENUS rescues demyelination from cisplatin treatment**

1056 (A) MBP (green), NF-09 (red) and DAPI (blue) staining of ACC area. Scale bar: 50 μ m. (B) Mean

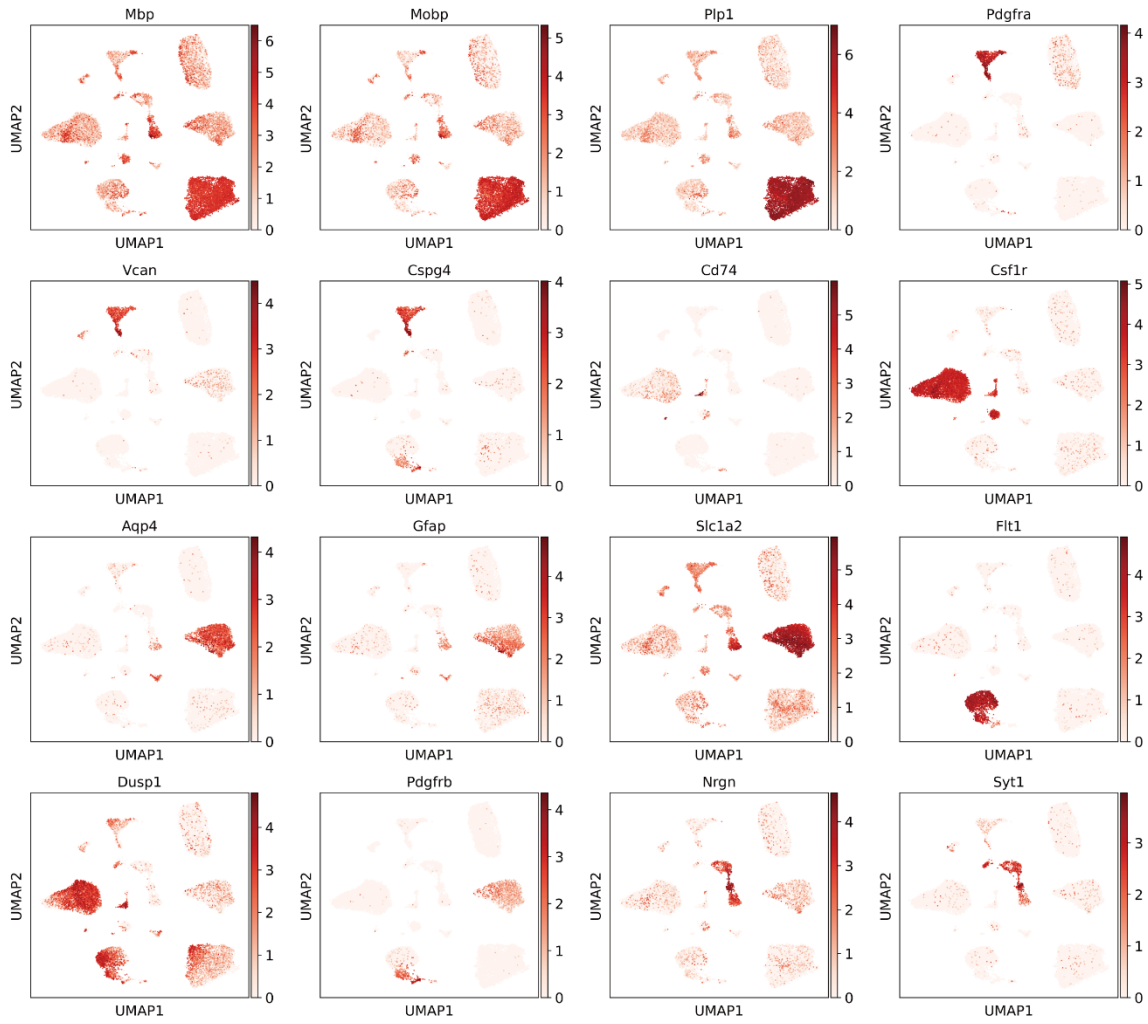
1057 value of area covered by myelin (PBS NS, n = 10; PBS S, n = 10; Cis NS, n = 10; Cis S, n = 12,

1058 Two-way ANOVA, Tukey's multiple comparison test). (C) MBP (green), NF-09 (red) and NeuN

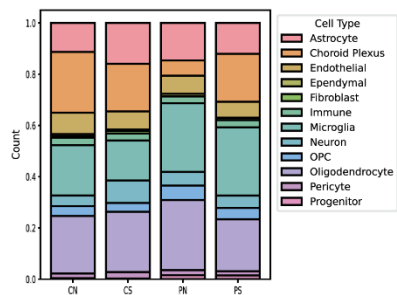
1059 (blue) staining of PFC area. Scale bar : 50 μ m. (D) Colocalization ratio of MBP signal with NF-09

1060 signal (PBS NS, n = 6; PBS S, n = 6; Cis NS, n = 6; Cis S, n = 6, Two-way ANOVA).

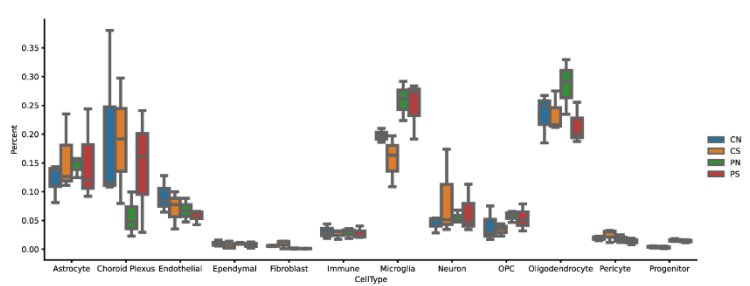
A



B

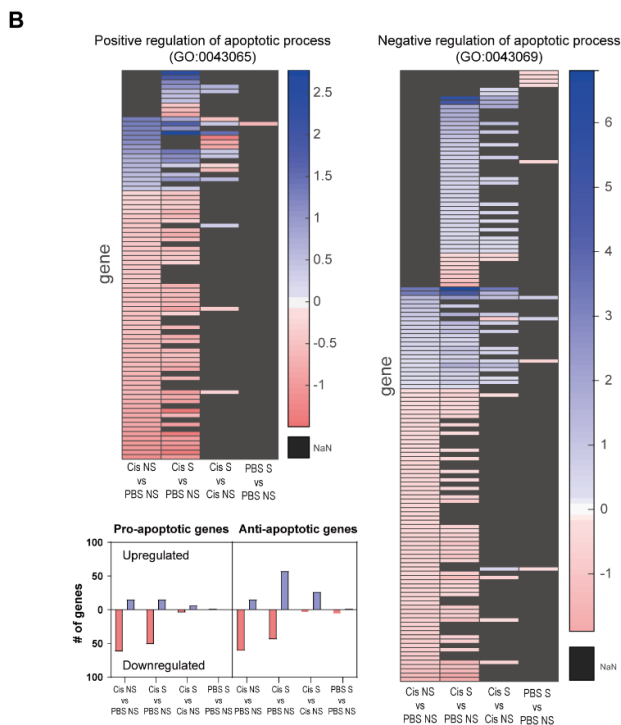
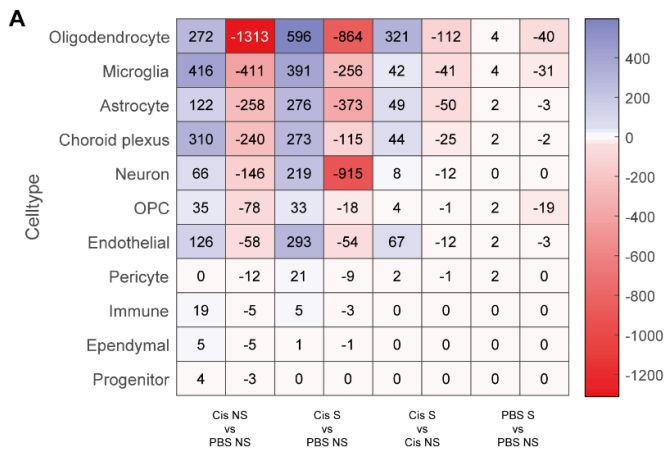


C



1062 **fig S6. Cell type markers and cell type distribution among each group.**

1063 (A) Expression pattern of each cell type marker used to classify cell type. (B) Cell type distribution
1064 for each treatment condition (Kruskal-Wallis test for cell type abundance across case-control, chi-
1065 squared = 0.021259, df = 3, p-value = 0.9992, or for cell abundance across cell types, chi-squared
1066 = 0.26022, df = 11, p-value = 1). (C) Cell type distribution in bar plot.



1067

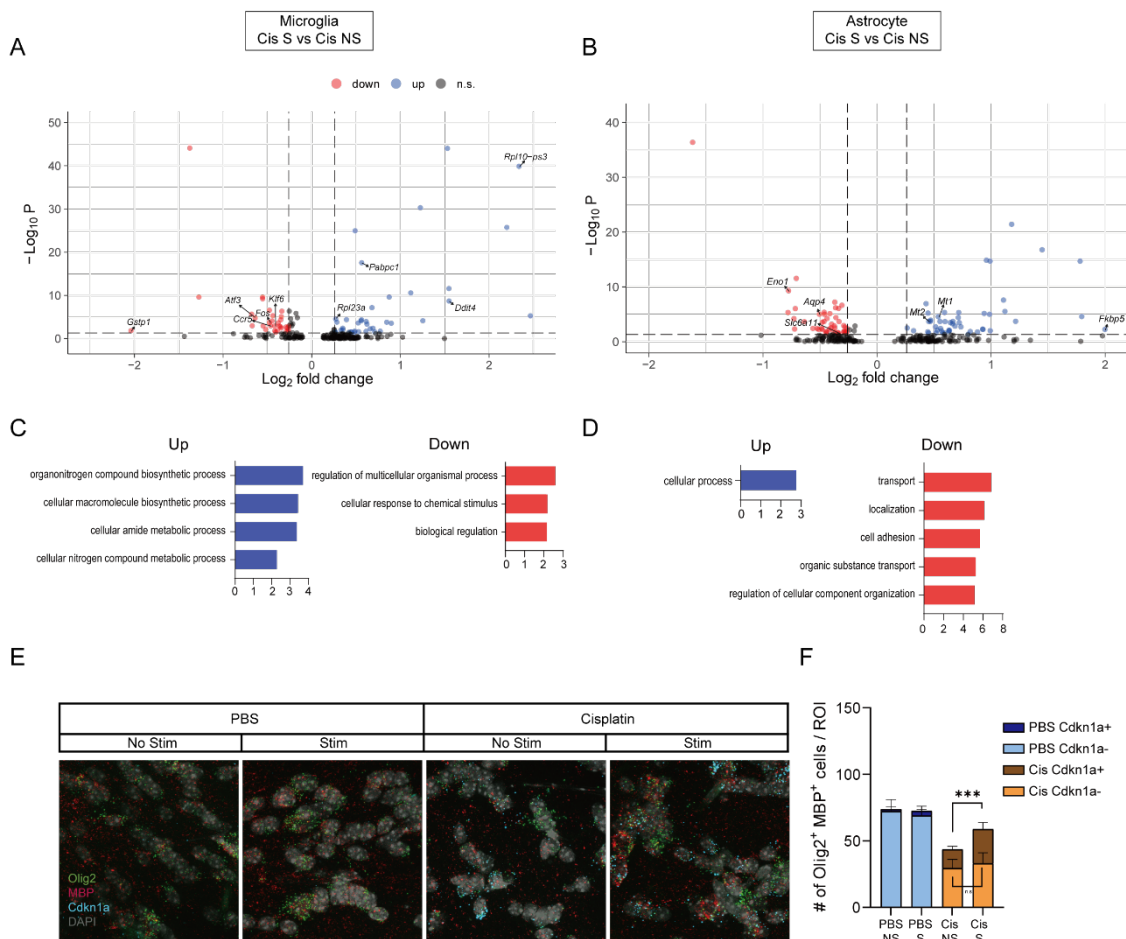
1068 **fig. S7. Cisplatin and GENUS alter gene expression in oligodendrocytes.**

1069 (A) Number of DEG across cell types and conditions. (B) Upregulated (blue) and downregulated

1070 (red) DEG in GO terms “Positive regulation of apoptotic process” and “Negative regulation of

1071 apoptotic process” in oligodendrocytes.

1072



1073

1074

1075 **fig. S8. Cisplatin and GENUS alter microglia and astrocyte gene expression**

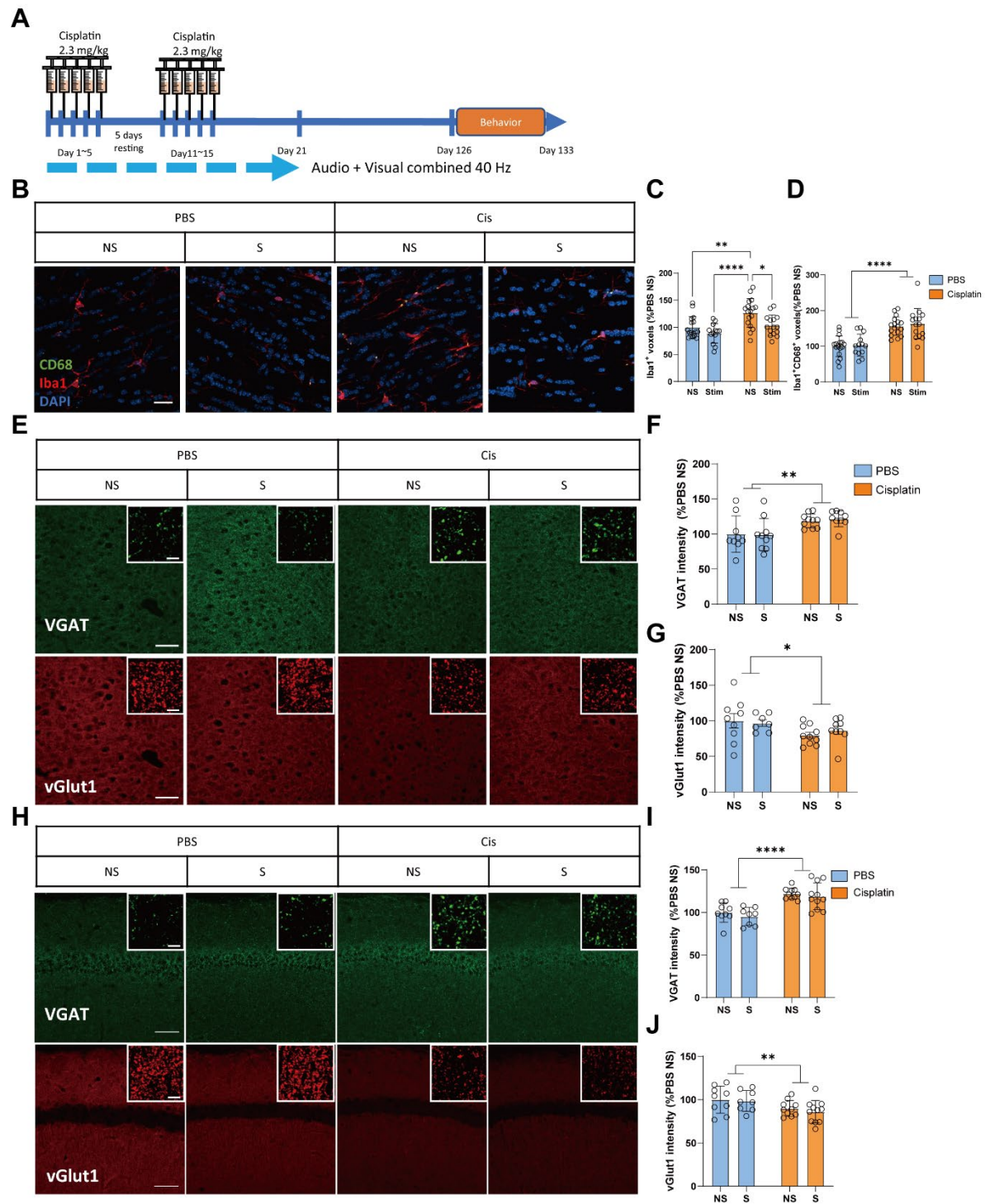
1076 (A) Volcano plot showing DEG between Cis NS and Cis S microglia. (B) Upregulated and

1077 downregulated GO terms in Cis S compared to Cis NS microglia. (C) Volcano plot showing DEG

1078 between Cis NS and Cis S astrocytes. (D) Upregulated and downregulated GO terms in Cis S

1079 compared to Cis NS astrocyte. (E) Olig2 (green), MBP (red), Cdkn1a (cyan) and DAPI (grey)

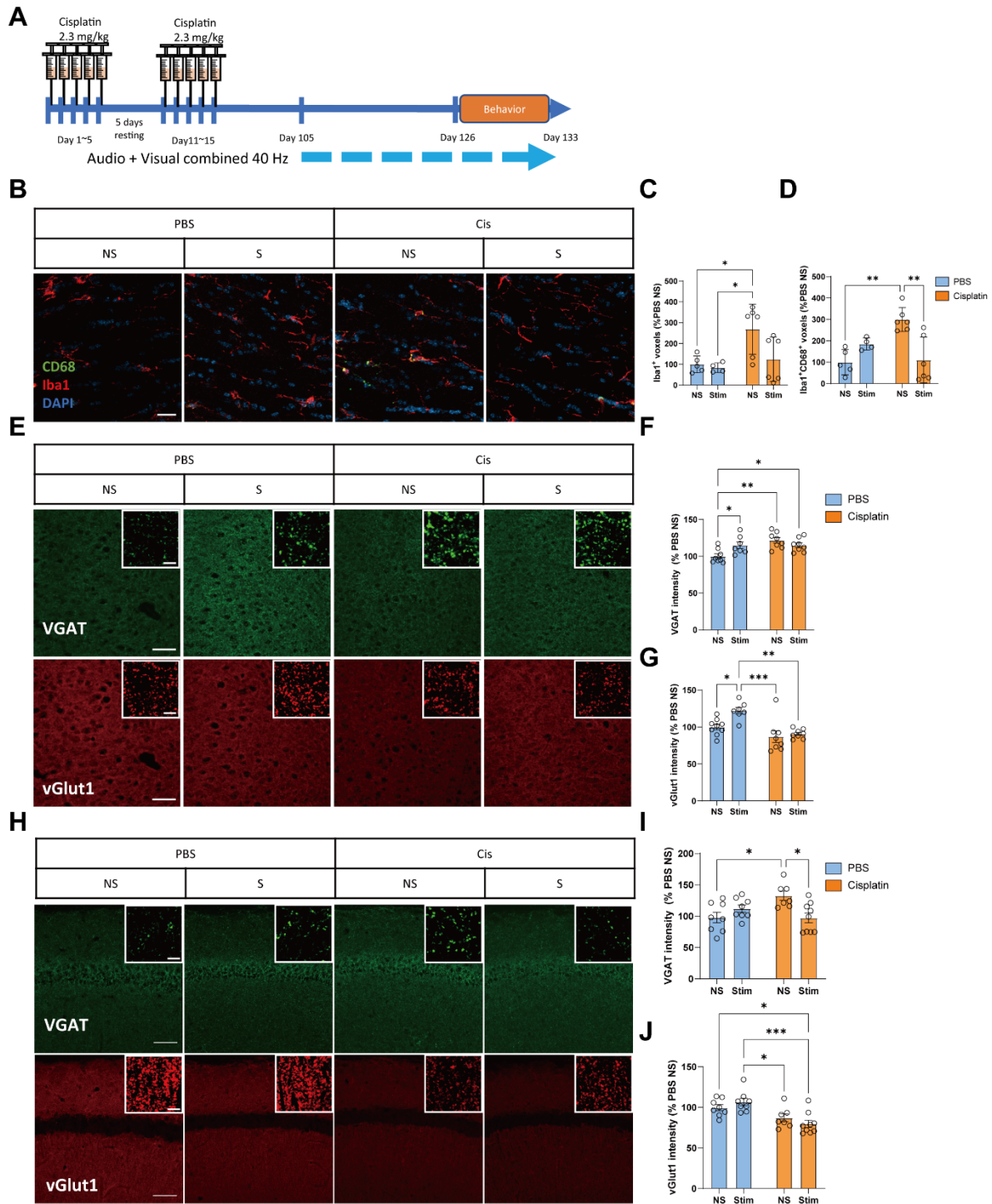
1080 FISH staining of corpus callosum area. (F) Number of Olig2⁺ MBP⁺ cells with or without Cdkn1a
1081 signal per mm² (PBS NS, n = 4; PBS S, n = 4; Cis NS, n = 4; Cis S, n = 4, two-way ANOVA,
1082 Tukey's multiple comparison test).



1084 **fig. S9. GENUS treatment during chemotherapy prevents progression of chemobrain**
1085 **pathology**

1086 **(A)** Drawing of experimental schematics. **(B)** Staining of CD68 (green), Iba1 (red) and DAPI (blue)
1087 in corpus callosum area. Scale bar: 20 μm **(C)** Mean value of Iba1⁺ voxels (PBS NS, n = 17; PBS
1088 S, n = 13; Cis NS, n = 17; Cis S, n = 15, Two-way ANOVA, Tukey's multiple comparison test).
1089 **(D)** Mean value of CD68⁺ / Iba1⁺ voxels (PBS NS, n = 17; PBS S, n = 13; Cis NS, n = 17; Cis S,
1090 n = 15, Two-way ANOVA, Tukey's multiple comparison test). **(E)** Staining of VGAT (green) and
1091 vGlut1 (red) of PFC area. Insert: 63x image of the PFC area. Scale bar: 50 μm (insert : 5 μm). **(F)**
1092 Mean value of VGAT signal intensity (PBS NS, n = 9; PBS S, n = 10; Cis NS, n = 10; Cis S, n =
1093 9, Two-way ANOVA, effect of cisplatin). **(G)** Mean value of vGlut1 signal intensity (PBS NS, n
1094 = 9; PBS S, n = 7; Cis NS, n = 10; Cis S, n = 9, Two-way ANOVA, effect of cisplatin). **(H)** Staining
1095 of VGAT (green) and vGlut1 (red) of CA1 area. Insert: 63x image of the CA1 area. Scale bar:
1096 50 μm (insert : 5 μm). **(I)** Mean value of VGAT signal intensity (PBS NS, n = 9; PBS S, n = 8;
1097 Cis NS, n = 10; Cis S, n = 11, Two-way ANOVA, effect of cisplatin). **(J)** Mean value of vGlut1
1098 signal intensity (PBS NS, n = 9; PBS S, n = 8; Cis NS, n = 10; Cis S, n = 11, Two-way ANOVA,
1099 effect of cisplatin).

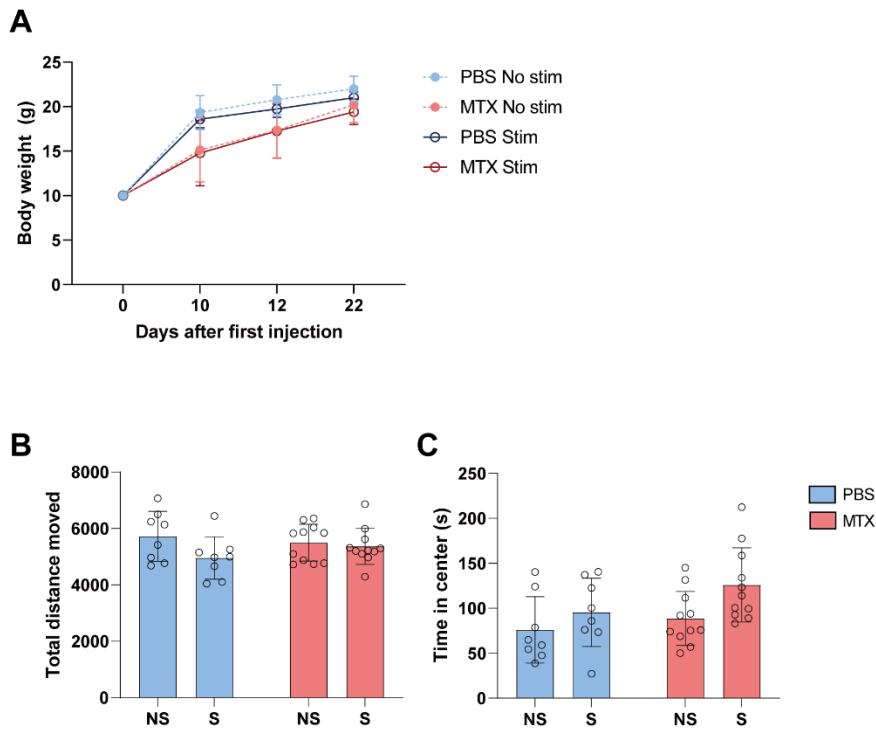
1100



1102 **fig. S10. Post-chemotherapy GENUS treatment has limited effect on chemobrain pathology**

1103 (A) Drawing of experimental schematics. (B) Staining of CD68 (green), Iba1 (red) and DAPI (blue)
1104 in corpus callosum area. Scale bar: 20 μm . (C) Mean value of Iba1⁺ voxels (PBS NS, n = 5; PBS
1105 S, n = 4; Cis NS, n = 6; Cis S, n = 6, Two-way ANOVA, Tukey's multiple comparison test). (D)
1106 Mean value of CD68⁺ / Iba1⁺ voxels (PBS NS, n = 5; PBS S, n = 4; Cis NS, n = 6; Cis S, n = 6,
1107 Two-way ANOVA, Tukey's multiple comparison test). (E) Staining of VGAT (green) and vGlut1
1108 (red) of PFC area. Insert: 63x image of the PFC area. Scale bar: 50 μm (insert : 5 μm). (F) Mean
1109 value of VGAT signal intensity (PBS NS, n = 8; PBS S, n = 7; Cis NS, n = 8; Cis S, n = 8, Two-
1110 way ANOVA, effect of cisplatin). (G) Mean value of vGlut1 signal intensity (PBS NS, n = 9; PBS
1111 S, n = 7; Cis NS, n = 8; Cis S, n = 8, Two-way ANOVA, effect of cisplatin). (H) Staining of VGAT
1112 (green) and vGlut1 (red) of CA1 area. Insert: 63x image of the CA1 area. Scale bar: 50 μm (insert :
1113 5 μm). (I) Mean value of VGAT signal intensity (PBS NS, n = 8; PBS S, n = 8; Cis NS, n = 7; Cis
1114 S, n = 9, Two-way ANOVA, effect of cisplatin). (J) Mean value of vGlut1 signal intensity (PBS
1115 NS, n = 8; PBS S, n = 8; Cis NS, n = 7; Cis S, n = 9, Two-way ANOVA, effect of cisplatin).

1116



1117

1118 **fig. S11. Body weight change and OFT results for MTX-induced chemobrain mouse model.**

1119 (A) Mean value of body weight from each animal during the experiment (PBS NS, n = 8; PBS S,

1120 n = 8; MTX NS, n = 7; MTX S, n = 7, Three-way ANOVA, effect of MTX ****P < 0.001). (B)

1121 Mean value of total distance moved during 10 min OFT (PBS NS, n = 8; PBS S, n = 8; MTX NS,

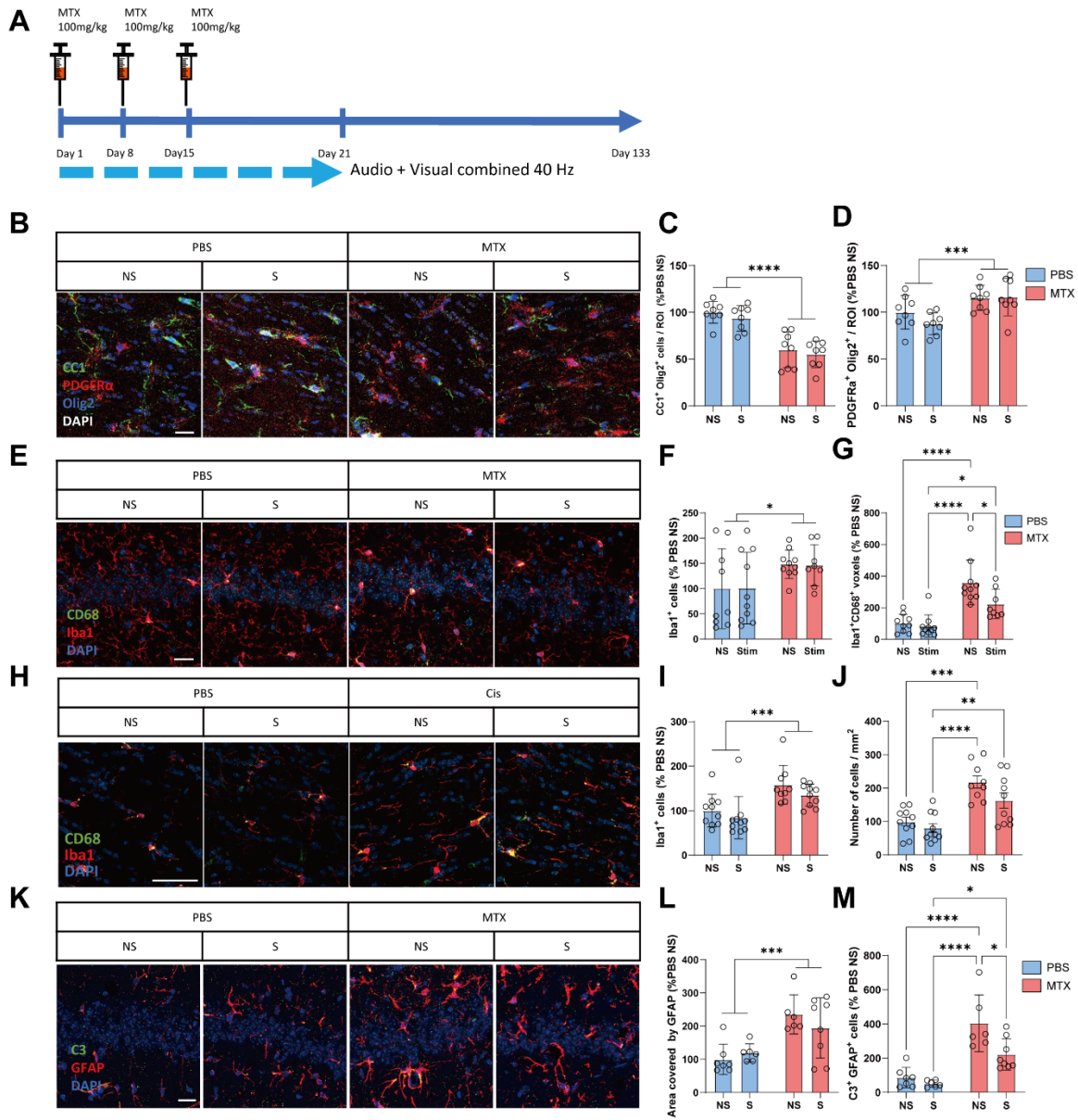
1122 n = 11; MTX S, n = 11, Two-way ANOVA). (C) Mean value of time spent in center area during

1123 10 min OFT (PBS NS, n = 8; PBS S, n = 8; MTX NS, n = 11; MTX S, n = 11, Two-way ANOVA,

1124 effect of GENUS *p < 0.05).

1125

1126



1128

1129 **fig. S12. GENUS treatment during chemotherapy reduces glial activation marker expression**
1130 **112 days post GENUS.**

1131 **(A)** Drawing of experimental timeline. **(B)** Staining of CC1 (green), PDGFR α (red), Olig2 (blue)
1132 and DAPI (grey) of corpus callosum area. Scale bar: 25 μ m. **(C)** Mean number of CC1⁺ Olig2⁺
1133 cells (PBS NS, n = 8; PBS S, n = 8; MTX NS, n = 8; MTX S, n = 8, Two-way ANOVA, effect of
1134 MTX). **(D)** Mean number of PDGFR α ⁺ Olig2⁺ (PBS NS, n = 8; PBS S, n = 8; MTX NS, n = 8;
1135 MTX S, n = 8, Two-way ANOVA, effect of MTX). **(E)** Staining of CD68 (green), Iba1 (red) and
1136 DAPI (blue) of corpus callosum area. Scale bar: 50 μ m. **(F)** Mean number of Iba1⁺ cells (PBS NS,
1137 n = 9; PBS S, n = 10; MTX NS, n = 10; MTX S, n = 8, Two-way ANOVA, effect of MTX). **(G)**
1138 Mean value of CD68⁺ / Iba1⁺ voxels (PBS NS, n = 9; PBS S, n = 10; MTX NS, n = 10; MTX S, n
1139 = 8, Two-way ANOVA, effect of MTX). **(H)** Staining of CD68 (green), Iba1 (red) and DAPI (blue)
1140 of CA1 area. Scale bar: 25 μ m. **(I)** Mean value of Iba1⁺ voxels (PBS NS, n = 10; PBS S, n = 10;
1141 MTX NS, n = 9; MTX S, n = 10, Two-way ANOVA, effect of MTX). **(J)** Mean value of CD68⁺ /
1142 Iba1⁺ voxels (PBS NS, n = 10; PBS S, n = 10; MTX NS, n = 9; MTX S, n = 10, Two-way ANOVA,
1143 effect of MTX). **(K)** Staining of C3 (green), GFAP (red) and DAPI (blue) of CA1 area. Scale bar:
1144 25 μ m. **(L)** Mean value of area covered by GFAP (PBS NS, n = 7; PBS S, n = 6; MTX NS, n = 6;
1145 MTX S, n = 8, Two-way ANOVA, effect of MTX). **(M)** Mean number of C3⁺ / GFAP⁺ cells (PBS
1146 NS, n = 7; PBS S, n = 6; MTX NS, n = 6; MTX S, n = 8, Two-way ANOVA, effect of MTX).

1147

1149 **fig. S13 GENUS treatment during MTX chemotherapy rescue inhibitory synaptic loss.**

1150 **(A)** Schematic drawing of experimental timeline. **(B)** Staining of VGAT (green) and vGlut1 (red)

1151 of PFC area. Insert: 63x image of the PFC area. Scale bar: 50 μm (insert : 5 μm). **(C)** Mean value

1152 of VGAT signal intensity (PBS NS, n = 12; PBS S, n = 10; MTX NS, n = 10; MTX S, n = 10,

1153 Two-way ANOVA, Tukey's multiple comparison test). **(D)** Mean value of vGlut1 signal intensity

1154 (PBS NS, n = 12; PBS S, n = 10; MTX NS, n = 10; MTX S, n = 10, Two-way ANOVA, Tukey's

1155 multiple comparison test). **(E)** Staining of VGAT (green) and vGlut1 (red) of CA1 area. Insert:

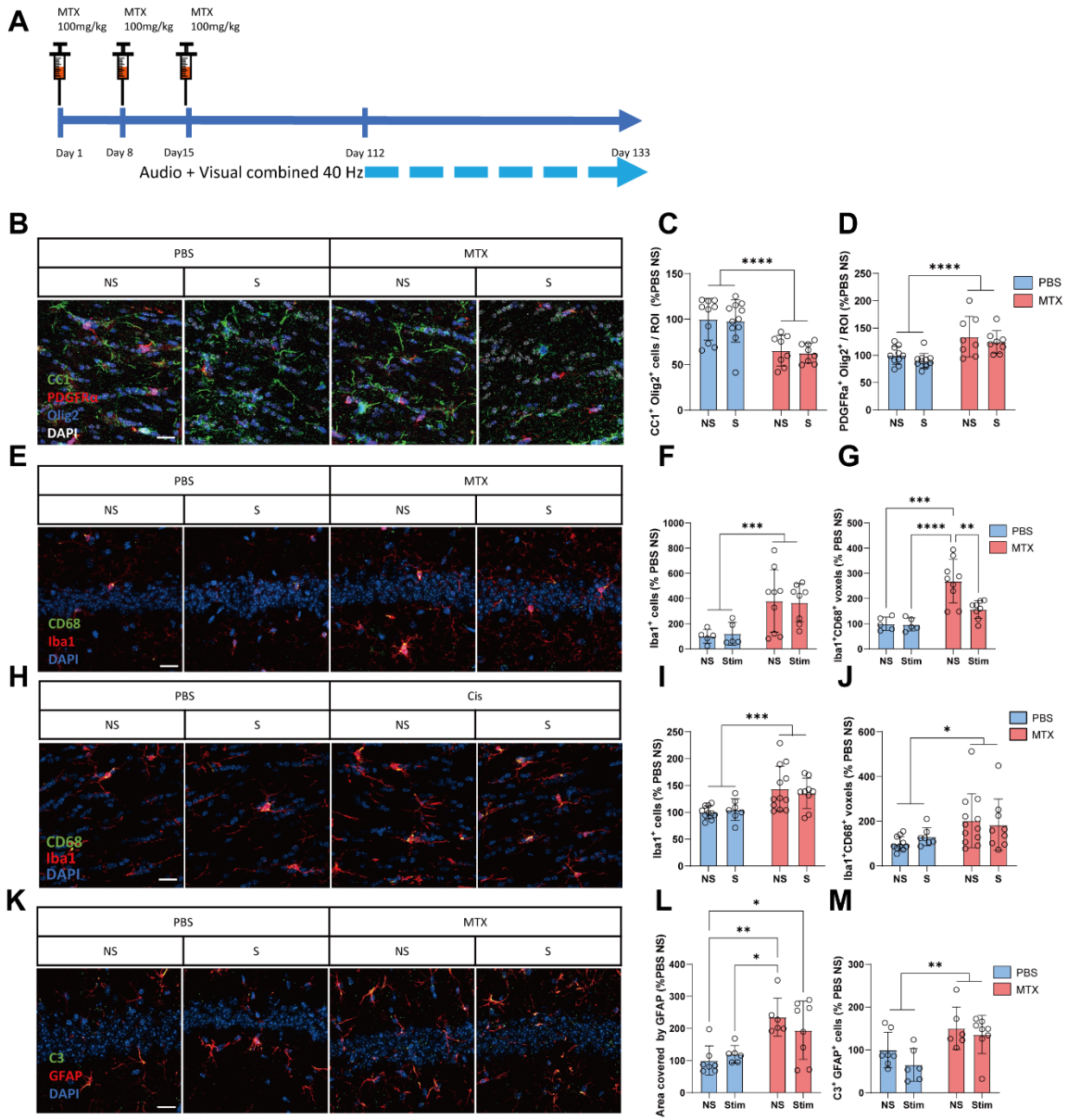
1156 63x image of the CA1 area. Scale bar: 50 μm (insert : 5 μm). **(F)** Mean value of VGAT signal

1157 intensity (PBS NS, n = 11; PBS S, n = 10; MTX NS, n = 10; MTX S, n = 10, Two-way ANOVA,

1158 Tukey's multiple comparison test). **(G)** Mean value of vGlut1 signal intensity (PBS NS, n = 11;

1159 PBS S, n = 10; MTX NS, n = 11; MTX S, n = 10, Two-way ANOVA, Tukey's multiple comparison

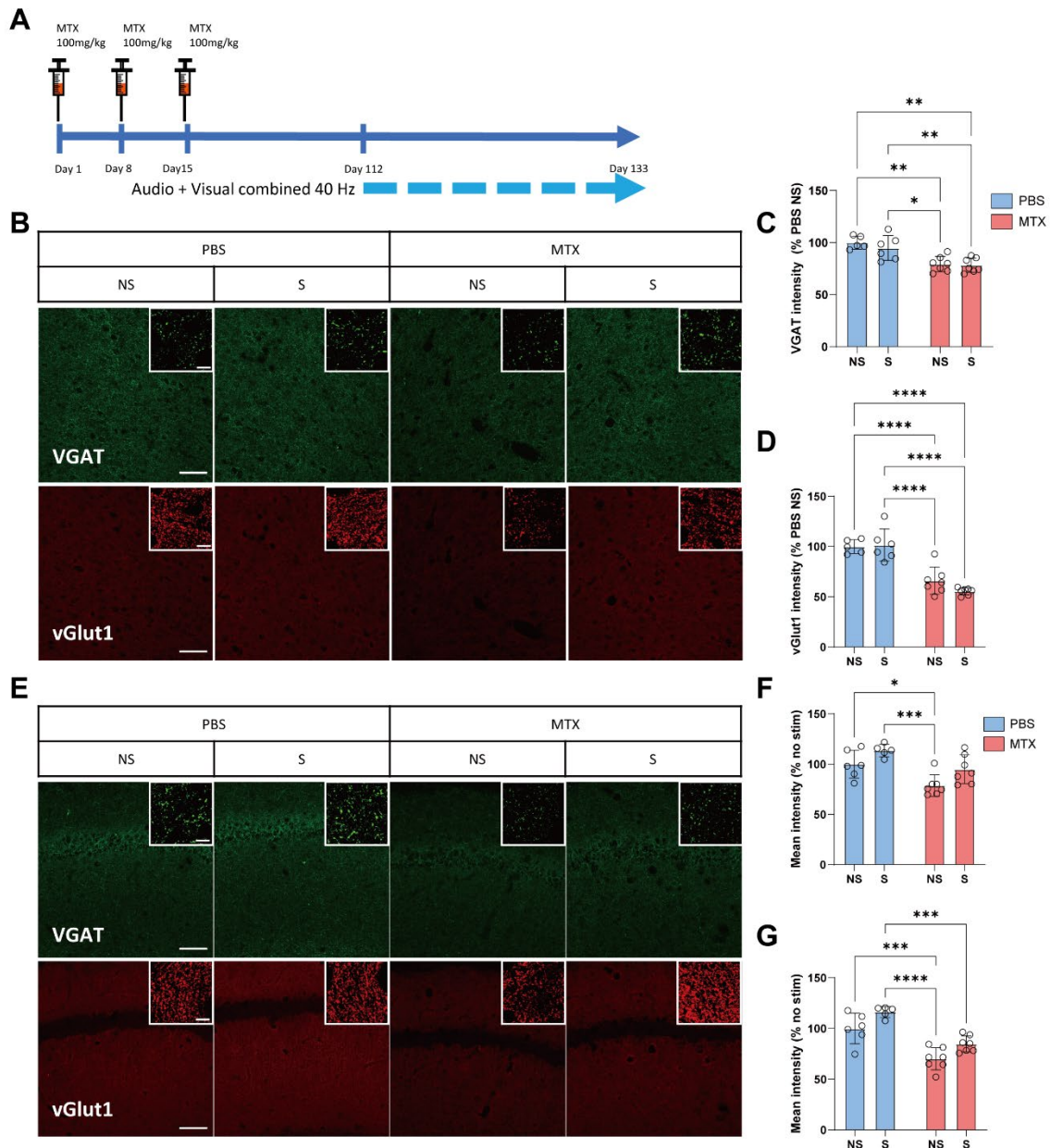
1160 test).



1162 **fig. S14 GENUS treatment post MTX chemotherapy does not rescue oligodendrocyte loss**
1163 **and has minimal effect on glial activation.**

1164 **(A)** Drawing of experimental timeline. **(B)** Staining of CC1 (green), PDGFR α (red), Olig2 (blue)
1165 and DAPI (grey) of corpus callosum area. Scale bar: 20 μ m. **(C)** Mean number of CC1⁺ / Olig2⁺
1166 cells (PBS NS, n = 10; PBS S, n = 11; MTX NS, n = 8; MTX S, n = 8, Two-way ANOVA, effect
1167 of MTX). **(D)** Mean number of PDGFR α ⁺ Olig2⁺ (PBS NS, n = 10; PBS S, n = 11; MTX NS, n =
1168 8; MTX S, n = 8, Two-way ANOVA, effect of MTX). **(E)** Staining of CD68 (green), Iba1 (red)
1169 and DAPI (blue) of corpus callosum area. Scale bar: 20 μ m. **(F)** Mean number of Iba1⁺ cells (PBS
1170 NS, n = 5; PBS S, n = 5; MTX NS, n = 9; MTX S, n = 8, Two-way ANOVA, effect of MTX). **(G)**
1171 Mean value of CD68⁺ / Iba1⁺ voxels (PBS NS, n = 5; PBS S, n = 5; MTX NS, n = 9; MTX S, n =
1172 8, Two-way ANOVA, effect of MTX). **(H)** Staining of CD68 (green), Iba1 (red) and DAPI (blue)
1173 of CA1 area. Scale bar: 20 μ m. **(I)** Mean value of Iba1⁺ voxels (PBS NS, n = 10; PBS S, n = 7;
1174 MTX NS, n = 12; MTX S, n = 9, Two-way ANOVA, effect of MTX). **(J)** Mean value of CD68⁺ /
1175 Iba1⁺ voxels (PBS NS, n = 10; PBS S, n = 7; MTX NS, n = 12; MTX S, n = 9, Two-way ANOVA,
1176 Tukey's multiple comparison test). **(K)** Staining of C3 (green), GFAP (red) and DAPI (blue) of
1177 CA1 area. Scale bar: 20 μ m. **(L)** Mean value of area covered by GFAP (PBS NS, n = 7; PBS S, n
1178 = 6; MTX NS, n = 6; MTX S, n = 8, Two-way ANOVA, Tukey's multiple comparison test). **(M)**
1179 Mean number of C3⁺ / GFAP⁺ cells (PBS NS, n = 7; PBS S, n = 6; MTX NS, n = 6; MTX S, n =
1180 8, Two-way ANOVA, effect of MTX).

1181



1183 **fig. S15 GENUS treatment post MTX chemotherapy rescue excitatory synaptic loss.**

1184 (A) Schematic drawing of experimental timeline. (B) Staining of VGAT (green) and vGlut1 (red)
1185 of PFC area. Insert: 63x image of the PFC area. Scale bar: 50 μm (insert : 5 μm). (C) Mean value
1186 of VGAT signal intensity (PBS NS, n = 5; PBS S, n = 6; MTX NS, n = 7; MTX S, n = 7, Two-
1187 way ANOVA, effect of MTX). (D) Mean value of vGlut1 signal intensity (PBS NS, n = 5; PBS S,
1188 n = 6; MTX NS, n = 7; MTX S, n = 7, Two-way ANOVA, Tukey's multiple comparison test). (E)
1189 Staining of VGAT (green) and vGlut1 (red) of CA1 area. Insert: 63x image of the CA1 area. Scale
1190 bar: 50 μm (insert : 5 μm). (F) Mean value of VGAT signal intensity (PBS NS, n = 6; PBS S, n =
1191 5; MTX NS, n = 7; MTX S, n = 7, Two-way ANOVA, Tukey's multiple comparison test). (G)
1192 Mean value of vGlut1 signal intensity (PBS NS, n = 6; PBS S, n = 5; MTX NS, n = 7; MTX S, n
1193 = 7, Two-way ANOVA, Tukey's multiple comparison test).

1194

Figure	Panel	Datapoint means	n				Analysis method	Data averaged
			PBS NS	PBS S	Cis NS	Cis S		
1	E	1 mouse	16	15	16	16	Two-way ANOVA, Tukey's multiple comparisons test	combined area of ventricles on each slice from 7 slices
1	G	1 mouse	8	6	7	5	Two-way ANOVA, Tukey's multiple comparisons test	two hemispheres each on two slices (total 4)
1	I	1 mouse	8	7	8	9	Two-way ANOVA, Tukey's multiple comparisons test	two hemispheres each on two slices (total 4)
1	J	1 mouse	8	7	8	9	Two-way ANOVA, Tukey's multiple comparisons test	two hemispheres each on two slices (total 4)
1	K	1 mouse	8	7	8	9	Two-way ANOVA, Tukey's multiple comparisons test	two hemispheres each on two slices (total 4)
1	L	1 axon	60	60	60	60	Two-way ANOVA, Tukey's multiple comparisons test	Two slices
1	M	1 mouse	4	4	4	4	Two-way ANOVA, Tukey's multiple comparisons test	Two slices
2	G	1 mouse	8	7	10	9	Two-way ANOVA, Tukey's multiple comparisons test	two hemispheres each on two slices (total 4)
3	B	1 mouse	8	8	8	7	Two-way ANOVA, Tukey's multiple comparisons test	two hemispheres each on two slices (total 4)
3	D	1 mouse	4	4	4	4	Two-way ANOVA, effect of cisplatin	two hemispheres each on two slices (total 4)
3	G	1 mouse	9	9	5	9	Two-way ANOVA, effect of cisplatin	two hemispheres each on two slices (total 4)
3	I	1 mouse	5	7	10	7	Two-way ANOVA, Tukey's multiple comparisons test	two hemispheres each on two slices (total 4)
4	B	1 mouse	8	8	7	7	Two-way ANOVA, Tukey's multiple comparisons test	1 mouse
4	C	1 mouse	8	8	7	7	Two-way ANOVA, Tukey's multiple comparisons test	1 mouse
4	E	1 mouse	8	7	8	8	Two-way ANOVA, Tukey's multiple comparisons test	1 mouse
4	G-I	1 mouse	8	8	7	7	Two-way ANOVA, Tukey's multiple comparisons test	1 mouse
5	B, C	1 mouse	9	9	15	15	Two-way ANOVA, Tukey's multiple comparisons test	two hemispheres each on two slices (total 4)
5	D	1 mouse	10	10	15	15	Two-way ANOVA, Tukey's multiple comparisons test	two hemispheres each on two slices (total 4)
5	E-G	1 mouse	9	9	15	15	Two-way ANOVA, Tukey's multiple comparisons test	two hemispheres each on two slices (total 4)
5	I	1 mouse	16	12	12	14	Two-way ANOVA, Tukey's multiple comparisons test	two hemispheres each on two slices (total 4)
5	K, L	1 mouse	12	10	13	12	Two-way ANOVA, Tukey's multiple comparisons test	two hemispheres each on two slices (total 4)
5	N, O	1 mouse	7	6	7	7	Two-way ANOVA, Tukey's multiple comparisons test	two hemispheres each on two slices (total 4)
5	Q, R	1 mouse	10	10	10	10	Two-way ANOVA, Tukey's multiple comparisons test	two hemispheres each on two slices (total 4)
6	B, C	1 mouse	8	8	8	8	Two-way ANOVA, Tukey's multiple comparisons test	two hemispheres each on two slices (total 4)
6	D	1 mouse	8	8	8	8	Two-way ANOVA, Tukey's multiple comparisons test	two hemispheres each on two slices (total 4)
6	E-G	1 mouse	8	8	8	8	Two-way ANOVA, Tukey's multiple comparisons test	two hemispheres each on two slices (total 4)
6	I	1 mouse	10	10	10	11	Two-way ANOVA, Tukey's multiple comparisons test	two hemispheres each on two slices (total 4)
6	K, L	1 mouse	8	8	10	11	Two-way ANOVA, Tukey's multiple comparisons test	two hemispheres each on two slices (total 4)
6	N	1 mouse	8	8	9	10	Two-way ANOVA, effect of cisplatin	two hemispheres each on two slices (total 4)
6	O	1 mouse	8	8	9	10	Two-way ANOVA, Tukey's multiple comparisons test	two hemispheres each on two slices (total 4)
6	Q, R	1 mouse	8	8	8	6	Two-way ANOVA, Tukey's multiple comparisons test	two hemispheres each on two slices (total 4)
7	E	1 axon	30	30	30	30	Two-way ANOVA, Tukey's multiple comparisons test	Two slices
7	G	1 mouse	12	11	10	10	Two-way ANOVA, Tukey's multiple comparisons test	two hemispheres each on two slices (total 4)
7	I	1 mouse	12	12	15	14	Two-way ANOVA, Tukey's multiple comparisons test	two hemispheres each on two slices (total 4)
7	J	1 mouse	7	6	7	7	Two-way ANOVA, Tukey's multiple comparisons test	two hemispheres each on two slices (total 4)
7	K	1 mouse	8	8	7	7	Two-way ANOVA, Tukey's multiple comparisons test	1 mouse
7	L-N	1 mouse	8	8	12	12	Two-way ANOVA, Tukey's multiple comparisons test	1 mouse
Supplementary Figure 1		1 mouse	8	8	7	7	Tree-way ANOVA, effect of cisplatin	1 mouse
Supplementary Figure 2	B	1 mouse	13	12	16	13	Two-way ANOVA, Tukey's multiple comparisons test	3 points on two slices (total 6)
Supplementary Figure 2	D	1 mouse	6	6	7	7	Two-way ANOVA, Tukey's multiple comparisons test	two hemispheres each on two slices (total 4)
Supplementary Figure 2	E	1 mouse	9	9	10	10	Two-way ANOVA, Tukey's multiple comparisons test	two hemispheres each on two slices (total 4)
Supplementary Figure 2	G	1 mouse	5	5	5	5	Two-way ANOVA, Tukey's multiple comparisons test	two hemispheres each on two slices (total 4)
Supplementary Figure 2	I	1 mouse	5	5	5	5	Two-way ANOVA, Tukey's multiple comparisons test	two hemispheres each on two slices (total 4)
Supplementary Figure 2	J	1 mouse	5	5	5	5	Two-way ANOVA, Tukey's multiple comparisons test	two hemispheres each on two slices (total 4)
Supplementary Figure 2	K	1 mouse	5	5	5	5	Two-way ANOVA, Tukey's multiple comparisons test	two hemispheres each on two slices (total 4)
Supplementary Figure 2	L	1 mouse	5	5	5	5	Two-way ANOVA, Tukey's multiple comparisons test	two hemispheres each on two slices (total 4)
Supplementary Figure 3	B	1 mouse	8	6	8	8	Two-way ANOVA, Tukey's multiple comparisons test	two hemispheres each on two slices (total 4)
Supplementary Figure 3	C	1 mouse	8	6	8	8	Two-way ANOVA, Tukey's multiple comparisons test	two hemispheres each on two slices (total 4)
Supplementary Figure 3	E	1 mouse	8	6	8	8	Two-way ANOVA, Tukey's multiple comparisons test	two hemispheres each on two slices (total 4)
Supplementary Figure 3	F	1 mouse	8	6	8	8	Two-way ANOVA, Tukey's multiple comparisons test	two hemispheres each on two slices (total 4)
Supplementary Figure 4	B, C	1 mouse	8	8	8	8	Two-way ANOVA, Tukey's multiple comparisons test	two hemispheres each on two slices (total 4)
Supplementary Figure 4	E, F	1 mouse	4	4	5	4	Two-way ANOVA, Tukey's multiple comparisons test	two hemispheres each on two slices (total 4)

Supplementary Figure 4	H, I	1 mouse	8	8	8	8	Two-way ANOVA, Tukey's multiple comparisons test	two hemispheres each on two slices (total 4)
Supplementary Figure 4	K, L	1 mouse	12	11	14	15	Two-way ANOVA, Tukey's multiple comparisons test	two hemispheres each on two slices (total 4)
Supplementary Figure 5	B	1 mouse	10	10	10	12	Two-way ANOVA, Tukey's multiple comparisons test	two hemispheres each on two slices (total 4)
Supplementary Figure 5	D	1 mouse	6	6	6	6	Two-way ANOVA	two hemispheres each on two slices (total 4)
Supplementary Figure 8	F	1 mouse	4	4	4	4	Two-way ANOVA, Tukey's multiple comparisons test	two hemispheres each on two slices (total 4)
Supplementary Figure 8	H	1 mouse	7	7	6	6	Two-way ANOVA, Tukey's multiple comparisons test	two hemispheres each on two slices (total 4)
Supplementary Figure 9	C, D	1 mouse	17	13	17	15	Two-way ANOVA, Tukey's multiple comparisons test	two hemispheres each on two slices (total 4)
Supplementary Figure 9	F	1 mouse	9	10	10	9	Two-way ANOVA, effect of cisplatin	two hemispheres each on two slices (total 4)
Supplementary Figure 9	G	1 mouse	9	7	10	9	Two-way ANOVA, effect of cisplatin	two hemispheres each on two slices (total 4)
Supplementary Figure 9	I, J	1 mouse	9	8	10	11	Two-way ANOVA, effect of cisplatin	two hemispheres each on two slices (total 4)
Supplementary Figure 10	C, D	1 mouse	5	4	6	6	Two-way ANOVA, Tukey's multiple comparisons test	two hemispheres each on two slices (total 4)
Supplementary Figure 10	F	1 mouse	8	7	8	8	Two-way ANOVA, effect of cisplatin	two hemispheres each on two slices (total 4)
Supplementary Figure 10	G	1 mouse	9	7	8	8	Two-way ANOVA, effect of cisplatin	two hemispheres each on two slices (total 4)
Supplementary Figure 10	I, J	1 mouse	8	8	7	9	Two-way ANOVA, effect of cisplatin	two hemispheres each on two slices (total 4)
Supplementary Figure 11	A	1 mouse	8	8	7	7	Three-way ANOVA, effect of MTX	1 mouse
Supplementary Figure 11	B, C	1 mouse	8	8	11	11	Two-way ANOVA	1 mouse
Supplementary Figure 12	C, D	1 mouse	8	8	8	8	Two-way ANOVA, effect of MTX	two hemispheres each on two slices (total 4)
Supplementary Figure 12	F, G	1 mouse	9	10	10	8	Two-way ANOVA, effect of MTX	two hemispheres each on two slices (total 4)
Supplementary Figure 12	I, J	1 mouse	10	10	9	10	Two-way ANOVA, effect of MTX	two hemispheres each on two slices (total 4)
Supplementary Figure 12	L, M	1 mouse	7	6	6	8	Two-way ANOVA, effect of MTX	two hemispheres each on two slices (total 4)
Supplementary Figure 13	C, D	1 mouse	12	10	10	10	Two-way ANOVA, Tukey's multiple comparisons test	two hemispheres each on two slices (total 4)
Supplementary Figure 13	F, G	1 mouse	11	10	10	10	Two-way ANOVA, Tukey's multiple comparisons test	two hemispheres each on two slices (total 4)
Supplementary Figure 14	C, D	1 mouse	10	11	8	8	Two-way ANOVA, effect of MTX	two hemispheres each on two slices (total 4)
Supplementary Figure 14	I, F	1 mouse	5	5	9	8	Two-way ANOVA, effect of MTX	two hemispheres each on two slices (total 4)
Supplementary Figure 14	J, G	1 mouse	5	5	9	8	Two-way ANOVA, Tukey's multiple comparisons test	two hemispheres each on two slices (total 4)
Supplementary Figure 14	I, J	1 mouse	10	7	12	9	Two-way ANOVA, effect of MTX	two hemispheres each on two slices (total 4)
Supplementary Figure 14	L	1 mouse	7	6	6	8	Two-way ANOVA, Tukey's multiple comparisons test	two hemispheres each on two slices (total 4)
Supplementary Figure 14	M	1 mouse	7	6	6	8	Two-way ANOVA, effect of MTX	two hemispheres each on two slices (total 4)
Supplementary Figure 15	C	1 mouse	5	6	7	7	Two-way ANOVA, effect of MTX	two hemispheres each on two slices (total 4)
Supplementary Figure 15	D	1 mouse	5	6	7	7	Two-way ANOVA, Tukey's multiple comparisons test	two hemispheres each on two slices (total 4)
Supplementary Figure 15	F, G	1 mouse	6	5	7	7	Two-way ANOVA, Tukey's multiple comparisons test	two hemispheres each on two slices (total 4)

1195

1196 **Supplementary table 1 Replicates and statistical analysis in figures.**

1197

1198